N-Benzyl 4,4-disubstituted piperidines as a potent class of influenza H1N1 virus inhibitors showing a novel mechanism of hemagglutinin fusion peptide interaction

Sonia de Castro,[a,1] Tiziana Ginex,[b,1] Evelien Vanderlinden,[c,1] Manon Laporte,[c] Annelies Stevaert,[c] José Cumella,[a] Federico Gago,[d] María José Camarasa,[a] F. Javier Luque,[b,*] Lieve Naesens,[c,*] and Sonsoles Velazquez[a,*]

[a] Instituto de Química Médica (C.S.I.C.), Juan de la Cierva 3, E-28006 Madrid, Spain

[b] Departament de Nutrició, Ciències de l'Alimentació I Gastronomia, Institut de Biomedicina (IBUB) and Institut de Química Teòrica i Computacional (IQTCUB), Facultat de Farmàcia i Ciències de l'Alimentació, Universitat de Barcelona, Santa Coloma de Gramenet, Spain

[c] Rega Institute for Medical Research, KU Leuven – University of Leuven, B-3000, Belgium

[d] Área de Farmacología, Departamento de Ciencias Biomédicas, Unidad Asociada al IQM-CSIC, Universidad de Alcalá, E-28805 Alcalá de Henares, Madrid, Spain

[*] Corresponding authors.

E-mail: iqmsv29@iqm.csic.es (SV), lieve.naesens@kuleuven.be (LN), fjluque@ub.edu (FJL)

[1] These authors contributed equally to this work.

ABSTRACT

The influenza virus hemagglutinin (HA) is an attractive target for antiviral therapy due to its essential role in mediating virus entry into the host cell. We here report the identification of a class of *N*-benzyl-4,4,-disubstituted piperidines as influenza A virus fusion inhibitors with specific activity against the H1N1 subtype. Using the highly efficient one-step Ugi four-component reaction, a diverse library of piperidine-based analogs was synthesized and evaluated to explore the structure-activity relationships (SAR). Mechanistic studies, including resistance selection with the most active compound (**2**) demonstrated that it acts as an inhibitor of the low pH-induced HA-mediated membrane fusion process. Computational studies identified an as yet unrecognized fusion inhibitor binding site, which is located at the bottom of the HA_2 stem in close proximity to the fusion peptide. A direct π-stacking interaction between the *N*-benzylpiperidine moiety of **2** and $F9_{HA2}$ of the fusion peptide, reinforced with an additional p-stacking interaction with $Y119_{HA2}$, and a salt bridge of the protonated piperidine nitrogen with $E120_{HA2}$, were identified as important interactions to mediate ligand binding. This site rationalized the observed SAR and provided a structural explanation for the H1N1-specific activity of our inhibitors. Furthermore, the HA_1-S326V mutation resulting in resistance to **2** is close to the proposed new binding pocket. Our findings point to the *N*-benzyl-4,4,-disubstituted piperidines as an interesting class of influenza virus inhibitors, representing the first example of fusion peptide binders with great potential for anti-influenza drug development.

KEYWORDS

Influenza virus, hemagglutinin, fusion peptide inhibitor, *N*-benzyl-4,4,-disubstituted piperidines

1. Introduction

Each year, influenza A and B viruses are responsible for 3-5 million severe cases and 290,000-650,000 deaths worldwide [1]. The death toll rises sharply during influenza pandemics, like the 2009 pandemic that was caused by a novel swine-origin A/H1N1 virus [2]. Though widely used and recommended, influenza vaccination is limited by suboptimal effectiveness, the need for annual injection and possibility of antigen mismatch [3]. The complementary strategy, antiviral therapy, is crucial to treat and prevent complicated influenza infections, which typically develop in aged, chronically ill or hospitalized individuals [4]. Nowadays, neuraminidase inhibitors are the only effective drug class that is widely available. Hence, there is an urgent need for new influenza blockers with a distinct mode of action. Some of these are under early or advanced clinical evaluation [5,6].

The trimeric hemagglutinin (HA) glycoprotein is an attractive drug target due to its critical and dual role in virus entry [7]: i) the HA globular head recognizes sialylated cell surface glycans and mediates virus attachment [8], and ii) HA is required for membrane fusion after the virus particles have entered by endocytosis. Upon acidification of the early into late endosomes, the low pH (~5) triggers radical refolding of HA, resulting in release of its hydrophobic fusion peptide and fusion of the viral and endosomal membranes [7]. Next, the viral genome segments traffic via the fusion pore into the nucleus to proceed with virus replication. Over the years, several HA inhibitors have been explored to target either the HA-host cell interaction through binding to the sialic acid binding pocket, or prevent the membrane fusion process with peptide and nonpeptide-based HA fusion inhibitors [9]. Since the low pH-induced refolding of HA involves the entire HA stem structure, HA fusion inhibitors may, at least in theory, target different HA binding pockets. Thus far, two major binding sites localized in the HA_1-HA_2 stem region have been identified and validated by structural data.

The first crystallographic structure of HA bound to a group 2-specific small fusion inhibitor, *tert*-butylhydroxyquinone (TBHQ; Fig. 1), was solved in 2008 [10]. TBHQ binds in a hydrophobic pocket located at the stem region of HA formed upon partial unfolding of the C-terminal region of the HA_2 B helix (site A in Fig. 1). This site is also targeted by arbidol (umifenovir; Fig. 1), a broad-spectrum antiviral compound approved in Russia and China [11], and by *N*-cyclohexyltaurine [12].

It was also proposed as the binding site for a class of group 1-specific aniline-based inhibitors (such as **9d** in Fig. 1; [13]). On the other hand, guided by the binding mode of the anti-HA stem antibody CR6261, the conserved HA_1-HA_2 fusion region of group 1 HAs is targeted by JNJ4796 (site B in Fig. 1; [14]), and the cyclic peptide CP141037 (not shown; [15]). Finally, MBX2329 and MBX2546 (Fig. 1) were found to inhibit group 1 A/H1N1 and A/H5N1 strains through binding to non-overlapping sites in the stem region of HA [16].

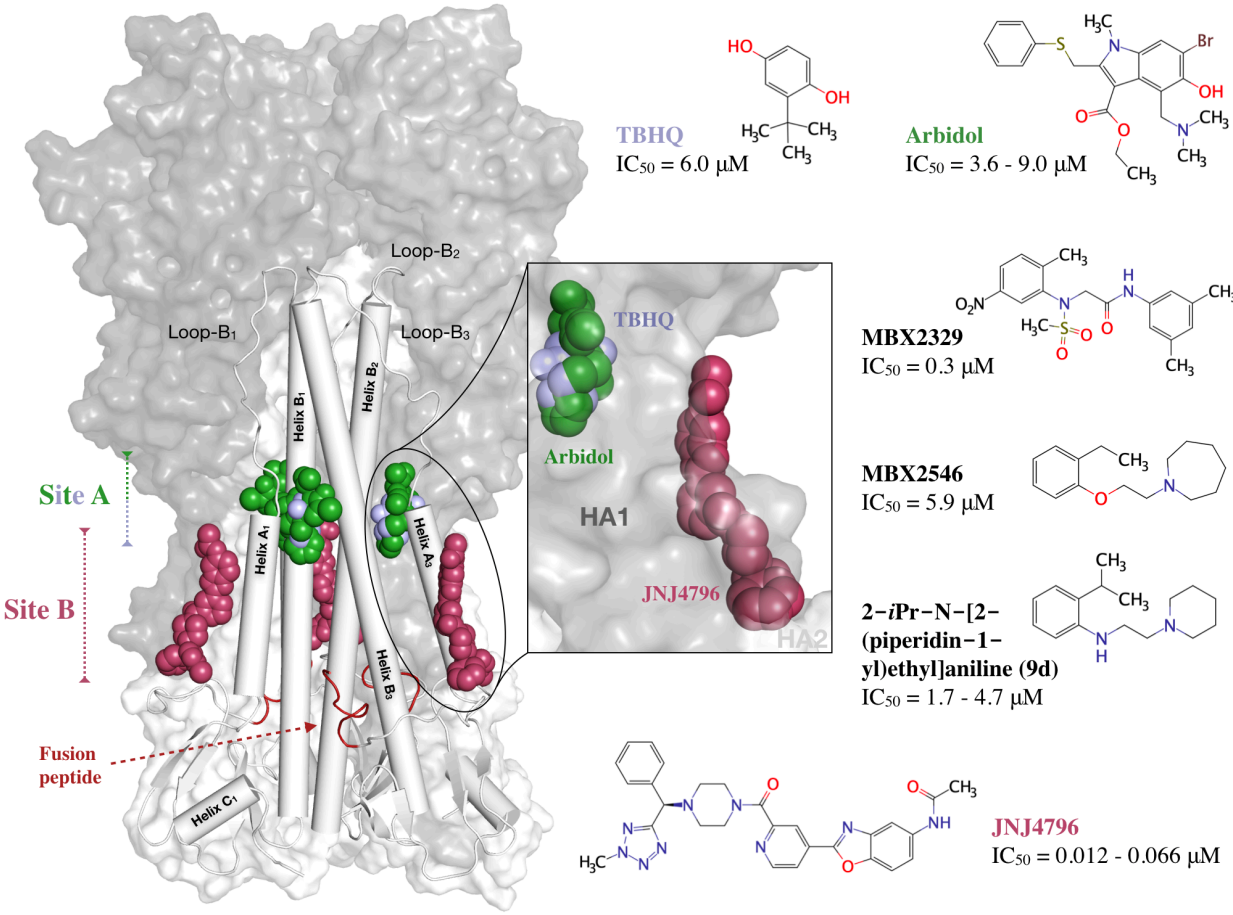

Fig. 1. Location of two known binding sites for HA fusion inhibitors. The site A binders TBHQ and arbidol are shown as blue and green spheres, respectively, while the site B binder JNJ4796 is displayed as magenta spheres. The fusion peptide is colored in red.

In this report, a novel class of piperidine-based HA fusion inhibitors is presented. The choice of a piperidine heterocycle was motivated by its pivotal role in drug design [17]. Recently reported

pharmacological uses of diverse substituted piperidine derivatives include coronary heart disease, anticancer, antivirals, and antinociceptives, among others [18-22]. In fact, one of the most frequently used non-aromatic ring systems in small molecule drugs is the piperidine ring [23], particularly 1,4-disubstituted piperidine, due to its easy synthesis and lack of stereochemical issues. A few years ago, we described [24] a structurally distinct series of 1,4,4-substituted piperidine derivatives, which were efficiently synthesized by means of the Ugi four-component reaction. These compounds of general formula **I** can be easily generated from amines, isocyanides, *N*-substituted piperidones and amino acids as ketone and carboxylic components (Fig. 2A). Hence, starting from commercially available reagents, five points of diversity can be introduced in a one-step reaction.

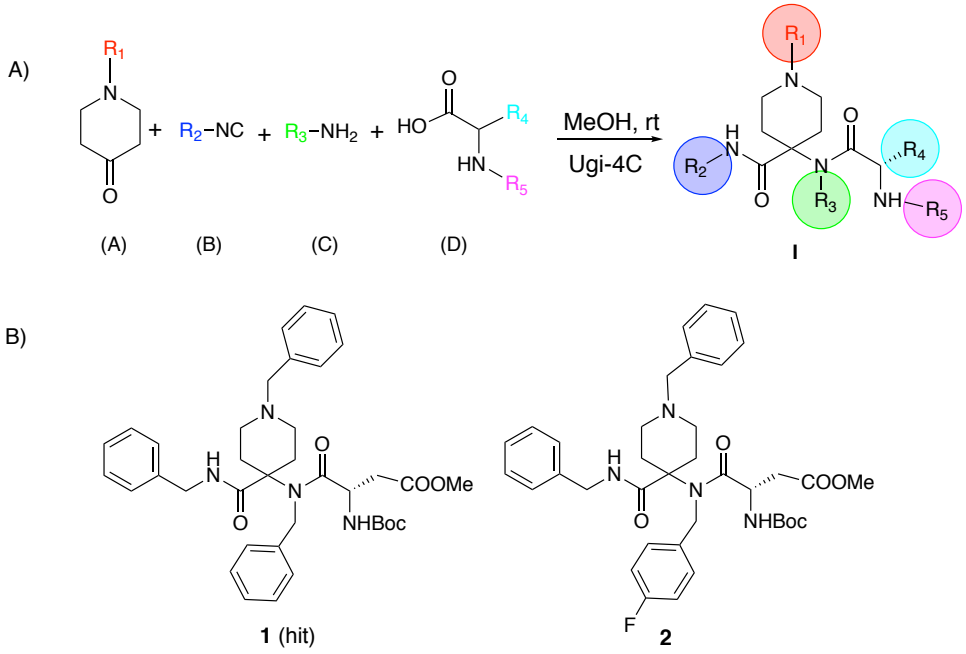

Fig. 2. Synthesis and chemical structures of 1,4,4-trisubstituted piperidine-based compounds. (A) Synthetic pathway of the target compounds **I** by Ugi-4C reaction. (B) Chemical structures of prototype compound **1** (hit) and its fluorine analogue **2**.

During broad biological evaluation, we noticed that **1** (Fig. 2B) exhibited low micromolar activity against influenza A/H1N1 virus. Starting from this hit compound, we here report the synthesis of an extended series of analogues to understand the structure-activity relationships (SAR) and explore the

antiviral mechanism of action. The most active compound, i.e. the fluorine derivative **2** (Fig. 2B), was selected for mechanistic studies including selection of resistant influenza virus mutants and influenza HA polykaryon assays. The biological findings were rationalized by *in silico* predictions of the binding mode within the viral HA protein, using molecular simulations. A new binding pocket that is located close to the fusion peptide at the HA_2 subunit is proposed. To the best of our knowledge, this pocket has not been so far explored by any inhibitors targeting the HA-mediated fusion process. Overall, the results show that the *N*-benzyl 4,4-disubstituted piperidine compounds represent a structurally promising scaffold for the design of influenza virus fusion inhibitors.

2. Results and Discussion

2.1. Chemistry

The Ugi four-component reaction is one of the most prominent isocyanide-based multicomponent reactions due to its versatility, atom economy and experimental simplicity, enabling the conversion of isocyanides, amines, aldehydes (ketones) and carboxylic acid into a great variety of bis-amide derivatives [25-27]. We previously applied this reaction for the efficient synthesis of a structurally diverse library of 1,4,4-substituted piperidine bis-amide derivatives (Fig. 2A; [24]). Antiviral evaluation of these compounds allowed us to identify the *N*-benzyl 4,4-dipeptide piperidine analogue **1** (Fig. 2B) as a promising hit endowed with low micromolar activity against influenza A/PR/8/34 (A/H1N1) virus. The inhibitory activity was even 5-fold higher for the 4-fluorobenzyl analogue **2** (Fig. 2B). Hence, we decided to synthesize a large series of piperidine-based analogues by modifying the R_1-R_5 substituents and investigating the SAR for influenza virus.

The general synthetic route for these novel piperidine analogues is depicted in Fig. 2A. The synthesis was accomplished in a relatively easy way via the Ugi four-component reaction with moderate to good yields. Commercially available *N*-substituted 4-piperidone (A), isocyanides (B), aromatic and aliphatic primary amines (C) and a variety of polar, hydrophobic or aromatic natural L-amino acids as carboxylic acids (D) were allowed to react in methanol at room temperature over 72 h, followed by chromatographic purification. In this work, 27 novel piperidine analogues were synthesized, fully

characterized as the corresponding free amine derivatives, and evaluated for antiviral activity. Using the Sirius T3 apparatus (Supplementary Material Fig. S1), a p*Ka* value of 7.5 was measured for compound **2**, indicating that its piperidine moiety should be positively charged at the acidic pH (~5) of late endosomes. We also evaluated the chemical stability at this acidic pH for the *N*-Boc or *N*-Cbz groups in the most active compounds **2** and **34**. They proved very stable after 72 h incubation in acetonitrile:acetate acidic buffer solutions (pH=5.5), which mimic the acidic conditions in the endosomal lumen.

2.2. Analysis of anti-influenza virus activity

Compounds **1** and **2** served as the starting points for an extensive SAR exploration against influenza virus, performed in MDCK cells infected with strain A/PR/8/34 (A/H1N1). For analysis of the antiviral results (Table 1), the compounds were organized in three subseries with modifications at i) R_1 or R_2, ii) R_3, and iii) R_4 or R_5.

In the first subseries, which comprises compounds retaining the 4-fluorobenzyl unit of **2**, the effect of R_1 and R_2 substituents was assessed using a variety of commercially available *N*-substituted piperidones (A) and isocyanides (B). Elimination of the *N*-1-benzylpiperidine nucleus (**3**) resulted in complete loss of activity. The antiviral activity was significantly reduced when the R_1 benzyl was missing (**4**) or replaced by cyclohexyl (**6**) or methyl (**5**), and totally lost in analogues having a cyclohexyl (**6**), phenyl, 4-Cl-phenyl or phenylethyl at R_1 (**7** and **8**). Thus, an *N*-1-benzyl piperidine substituent at R_1 was absolutely required for activity. Also, the R_2 benzyl group proved to be critical since its replacement by cyclohexyl (**9**), *t*-butyl (**10**) or tosylmethyl (**11**) was detrimental.

In the second subseries, the influence of the R_3 substituent was investigated by varying the nature of the primary amine (C). Again, the benzyl moiety appeared a critical structural element since its elimination (**12**) or replacement by alkyl (**14**), cyclopropyl (**15**) or phenylaminoethyl group (**16**) was detrimental for the inhibitory activity, while a methyl substituent was partially (**13**) tolerated. Besides, various substituents with different electronic properties were introduced at the R_3 aromatic substituent. At position 4, a halogen was clearly preferred (cfr. 5-fold higher activity of **2** compared to **1**), since the analogues carrying a methyl (**17**) or nitro group (**19**) were less active, while trifluoromethyl

(**18**) was detrimental. In line with the positive effect of the 4-F atom, even slightly higher potency was seen with the 4-chloro analogue **20**. The 2-F derivative was equipotent to the unsubstituted compound **1**, while a 3-F atom had intermediate effect. The 3,4-disubstituted fluoro compound **23** was inactive.

Finally, the third subseries explored changes at R_4 (mostly NHBoc or NHCbz) and R_5, including a variety of polar, hydrophobic or aromatic natural L-amino acid substituents. Substitution at R_4 proved advantageous yet not absolutely required (**25**). The difference between NHBoc and NHCbz was not clear, since NHBoc was preferred in one case (compare **2** to **26**) while NHCbz was superior in another case (compare **34** to **1**). An amino group at R_4 yielded a compound (**24**) with strong antiviral activity but pronounced cytotoxicity; hence, this substitution was not further explored. Regarding the R_5 group in Boc-protected amino acids, the antiviral potency was reduced by a factor of 5 when the Asp(OMe) [= CH_2COOMe] moiety in lead compound **2** was replaced by Ala (**27**) or Glu(OMe) [= CH_2CH_2COOMe] (**28**). Whereas replacing the Asp(OMe) by Asn [= CH_2CONH_2] did not alter the antiviral potency (**31** and **33**), a detrimental effect was seen when the methyl ester was hydrolysed to free acid (Asp **30**; $R_5 = CH_2COOH$). An alkyl (Ile **32**) or an aromatic (Phe **29**) moiety at R_5 was not tolerated in these close analogues of prototypes **1** and **2**. Remarkably, a different SAR trend was seen in the compound series with a cyclopropyl at R_3, since the Asp(OMe) analogue **34** was only 2- to 4-fold more active than the three analogues **35-37** with a hydrophobic alkyl (**35** and **36**) or an aromatic R_5 moiety (Phe **37**). Besides, derivatives **36** and **37** represent the only active compounds with an alkyl substituent at R_2 (*t*-butyl).

The window between activity and cytotoxicity was estimated by calculating the ratio between CC_{50} and EC_{50}, defined as the selectivity index (SI). The compounds showing superior selectivity were **34** [SI: 40], **31** [SI: 26], **2** [SI: 18], **35** [SI: 8] and **36** [SI: 13]. *Vice versa*, the following compounds proved quite active ($EC_{50} < 10$ μM) yet less selective [$SI \leq 10$]: **1**, **33**, **37**, **35**, **28**, **20**, **22** and **21**. The most cytotoxic compounds proved to be the 4-Cl benzyl analogue **20** and the R_4 deprotected free amine derivative **24** with CC_{50} values < 10 μM (compare with **2**).

Table 1. Antiviral activity and cytotoxicity of *N*-benzyl 4,4-disubstituted piperidine analogues of prototype compounds **1** and **2** in influenza A/H1N1 virus-infected MDCK cells.

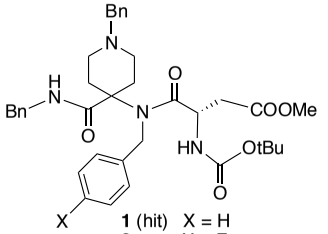

1 (hit) X = H
2 X = F

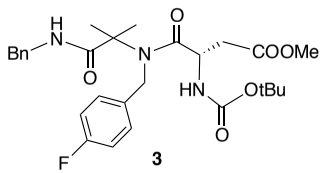

3

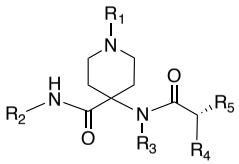

4-39

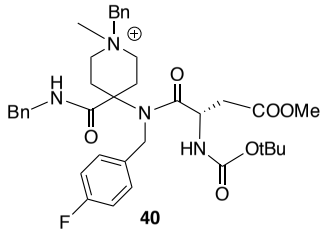

40

Compound	R_1	R_2	R_3	R_4	R_5	**Antiviral EC_{50}** (μM)[a] Influenza A/PR/8/34		**Cytotoxicity** (μM)[b]	
						CPE	MTS	MCC	CC_{50}
Original hit compounds									
1	Bn	Bn	Bn	NHBoc	CH_2COOMe	9.3 ± 0.7	10 ± 2	100 ± 0	56 ± 5
2	Bn	Bn	(4-F)Bn	NHBoc	CH_2COOMe	1.9 ± 0.1	2.7 ± 0.4	79 ± 9	49 ± 2
Subseries 1 (modifications at R_1 or R_2)									
3	-	Bn	(4-F)Bn	NHBoc	CH_2COOMe	>100	>100	>100	>100
4	H	Bn	(4-F)Bn	NHBoc	CH_2COOMe	≥73	≥89	>100	>100
5	Me	Bn	(4-F)Bn	NHBoc	CH_2COOMe	36 ± 8	36 ± 11	>100	>100
6	Chx	Bn	(4-F)Bn	NHBoc	CH_2COOMe	>100	> 100	20 ± 0	8.1 ± 0.5
7	Ph	Bn	(4-F)Bn	NHBoc	CH_2COOMe	>100	>100	≥100	>100
8	$(CH_2)_2Ph$	Bn	(4-F)Bn	NHBoc	CH_2COOMe	>100	>100	100 ± 0	59 ± 7
9	Bn	Chx	(4-F)Bn	NHBoc	CH_2COOMe	>100	>100	84 ± 15	58 ± 5
10	Bn	^{t}Bu	(4-F)Bn	NHBoc	CH_2COOMe	>100	>100	84 ± 15	73 ± 10
11	Bn	CH_2SO_2Ph -4-Me	(4-F)Bn	NHBoc	CH_2COOMe	>100	>100	100 ± 0	84 ± 10
Subseries 2 (modifications at R_3)									
12	Bn	Bn	H	NHBoc	CH_2COOMe	>100	>100	100 ± 0	55 ± 6

18	Bn	Bn	(4-CF_3)Bn	NHBoc	CH_2COOMe	>100	>100	17 ± 3	9.5 ± 0.7
19	Bn	Bn	(4-NO_2)Bn	NHBoc	CH_2COOMe	10 ± 4	>100	73 ± 27	42 ± 4
20	Bn	Bn	(4-Cl)Bn	NHBoc	CH_2COOMe	1.6 ± 0.3	1.6 ± 0.3	20 ± 0	8.2 ± 0.7
21	Bn	Bn	(2-F)Bn	NHBoc	CH_2COOMe	9.3 ± 0.4	8.7 ± 1.4	100 ± 0	41 ± 1
22	Bn	Bn	(3-F)Bn	NHBoc	CH_2COOMe	4.1 ± 1.8	5.2 ± 2.9	100 ± 0	44 ± 2
23	Bn	Bn	(3,4-F)Bn	NHBoc	CH_2COOMe	>100	>100	80 ± 20	50 ± 3
Subseries 3 (modifications at R_4 and/or R_5)									
24	Bn	Bn	(4-F)Bn	NH_2	CH_2COOMe	<0.8	<0.8	4 ± 0	6.4 ± 2.4
25	Bn	Bn	(4-F)Bn	H	CH_2COOMe	25 ± 11	24 ± 6	100 ± 0	85 ± 9
26	Bn	Bn	(4-F)Bn	NHCbz	CH_2COOMe	2.7 ± 1.3	>100	20 ± 0	25 ± 14
27	Bn	Bn	(4-F)Bn	NHBoc	CH_3	10 ± 1	11 ± 1	84 ± 16	53 ± 6
28	Bn	Bn	(4-F)Bn	NHBoc	$(CH_2)_2COOMe$	9.8 ± 1.2	10 ± 1	84 ± 16	56 ± 5
29	Bn	Bn	(4-F)Bn	NHBoc	Bn	>100	>100	14 ± 4	68 ± 20
30	H	Bn	(4-F)Bn	NHBoc	CH_2COOH	>100	>100	>100	>100
31	Bn	Bn	(4-F)Bn	NHBoc	CH_2CONH_2	1.8 ± 0.2	2.1 ± 0.5	84 ± 16	54 ± 4
32	Bn	Bn	Bn	NHBoc	CH(Me)(Et)	>100	>100	20	>100
33	Bn	Bn	Bn	NHBoc	CH_2CONH_2	6.3 ± 2.0	6.7 ± 1.7	100 ± 0	63 ± 8
34	Bn	Bn	Cyclopropyl	NHCbz	CH_2COOMe	2.0 ± 0.2	1.8 ± 0.1	20 ± 0	72 ± 28
35	Bn	Bn	Cyclopropyl	NHCbz	CH(Me)(Et)	5.1 ± 2.0	9.0 ± 0.8	47 ± 27	75 ± 16
36	Bn	tBu	Cyclopropyl	NHCbz	CH(Me)(Et)	4.3 ± 1.5	3.9 ± 0.9	20 ± 0	52 ± 10
37	Bn	tBu	Cyclopropyl	NHBoc	Bn	5.8 ± 1.8	5.3 ± 1.5	60 ± 18	54 ± 4
Molecular modeling-guided derivatives (modifications at R_1)									
38	3-F-$PhCH_2$	Bn	(4-F)Bn	NHBoc	CH_2COOMe	1.6 ± 0.1	1.6	16 ± 8	40
39	3,5-F-$PhCH_2$	Bn	(4-F)Bn	NHBoc	CH_2COOMe	>100	>100	2.6 ± 0	1.9 ± 0.1
40	-	Bn	(4-F)Bn	NHBoc	CH_2COOMe	>100	>100	>100	>100
Ribavirin						22 ± 4	31 ± 5	≥100	>100

[a] The EC_{50} represents the 50% effective concentration, or compound concentration producing 50% protection against virus-induced cytopathicity, as assessed by microscopic scoring of the cytopathic effect (CPE) or by MTS cell viability assay.

[b] Cytotoxicity expressed as the minimum cytotoxic concentration (MCC), i.e. compound concentration producing minimal microscopically visible changes in cell morphology; or CC_{50}, i.e. 50% cytotoxic concentration in the MTS cell viability assay.

Values shown are the mean ± SEM (N ≥ 3).

When the effect was determined on a panel of influenza A and B viruses (data not shown), the inhibition proved limited to the A/PR/8/34 strain. No activity was observed against pandemic 2009 virus (which alike A/PR/8/34 belongs to the A/H1N1 subtype), nor the A/H3N2 subtype and influenza B virus. On the other hand, compound **2** proved also effective in A/PR/8/34-infected Calu-3 cells, which are a relevant model for human airway epithelial cells. Namely, the anti-influenza virus EC_{50} value in Calu-3 cells was 1.8 μM based on CPE scoring and 3.0 μM when assessed by MTS assay (data not shown).

2.3. Mechanism of inhibitory activity

The most active compound **2** was selected for mechanistic investigations, starting with one-cycle time-of-addition experiments. Compound addition time was varied relative to virus infection and the reduction in viral vRNA synthesis was monitored at 10 h p.i. The influenza virus entry process consists of virus binding to the cells, uptake in and release from acidic endosomes, and import of viral ribonucleoprotein (vRNP) complexes into the nucleus, in total taking about 1 h in MDCK cells [28]. Hence, the reference compound chloroquine, which acts by increasing the endosomal pH, completely lost its activity when added at 1 h p.i. (Fig. 3). For ribavirin, an inhibitor of viral RNA synthesis [29], the time-of-addition curve was situated beyond 1 h p.i. with the steepest part between 3 and 5 h p.i. Nucleozin remained fully effective when added as late as 5 h p.i., consistent with the finding that late addition of this agent blocks cytoplasmic traffic of the vRNPs after their nuclear export [30]. For **2**, the curve fully overlapped with that of chloroquine, indicating that its action takes place during the endosomal stage of the virus. The low pH inside the endosomes triggers membrane fusion induced by HA, virus uncoating that requires M2 proton channel activity, and weakening of the vRNP-M1 matrix protein interactions.

To better define the target, influenza A/PR/8/34 virus was serially passaged in the absence or presence of **2**. Resistant virus emerging at passage #7 was plaque-purified and virus clones were submitted to phenotypic and genotypic analysis. As shown in Table 2, the two clones selected under **2** displayed manifest (>40-fold) resistance to **2** while being fully sensitive to ribavirin. Both clones contained no changes in the M1 and M2 proteins. As for HA, substitution HA_1-I324T is likely irrelevant

since it was previously detected upon passaging of A/PR/8/34 virus in cell culture and linked to polymorphism or cell culture adaptation [32]. The resistance to **2** was thus attributed to substitutions HA_1-S326V and HA_2-L99F. This concurred with its HA-subtype dependent activity and, in combination with the time-of-addition data, suggested that it affects HA-mediated membrane fusion.

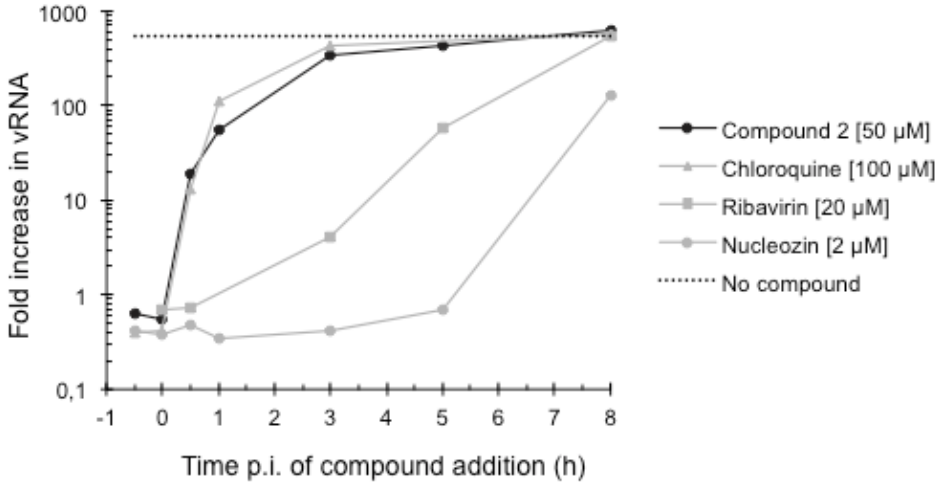

Fig. 3. Time-of-addition experiments showed that **2** acts during the endosomal stage in influenza virus entry. MDCK cells were infected with A/PR/8/34 virus and the compounds were added at different time points ranging from -0.5 h until 8 h p.i. At 10 h p.i., total cellular RNA extracts were prepared and viral vRNA was quantified by two-step RT-qPCR. The Y-axis shows the fold increase in vRNA relative to the amount added at time zero; the dashed line indicates the increase in the untreated virus control. Data are the mean of two independent experiments.

Table 2. Characterization of compound **2**-resistant mutant influenza viruses.

Virus/clone[a]	Residue substitutions[b]	Hemolysis pH[c]	Antiviral EC_{50} (µM)[d]			
			2		Ribavirin	
			CPE	MTS	CPE	MTS
2/cl1	HA_1-I324T HA_1-S326V HA_2-L99F	5.3 ± 0.0	>100	>100	11 ± 0	20 ± 2
2/cl2	HA_1-I324T HA_1-S326V HA_2-L99F	ND	>100	>100	13 ± 2	21 ± 3
No cpd/cl1	HA_2-T54A	5.3 ± 0.0	4.5 ± 0.1	13 ± 7	15 ± 2	22 ± 3
Parent virus[e]	-	5.0 ± 0.0	1.9 ± 0.1	2.7 ± 0.4	22 ± 4	31 ± 5

[a] A/PR/8/34 virus was serially passaged in MDCK cells in the absence of compound (no cpd control) or gradually increasing (up to 25 µM) concentrations of **2**. After seven passages, individual virus clones were obtained by plaque purification.
[b] Substitutions in HA relative to parent virus. Separate amino acid numbering for the HA_1 and HA_2 polypeptide parts of cleaved HA protein.

[c] pH at which 50% hemolysis occurs, relative to the value at pH 4.6.
[d] EC_{50}: 50% effective concentration, as determined by the microscopic CPE assay or MTS cell viability assay.
[e] Parent allantoic stock of A/PR/8/34 virus, used at the start of the passage experiment.
Values shown are the mean ± SEM (N ≥ 3). ND, not determined.

The precise mechanism was revealed in the polykaryon assay, which monitors cell-cell fusion that is provoked by influenza virus HA when its conformation changes at acidic pH. At a concentration of 100 μM, **2** completely inhibited polykaryon formation in H1 (A/PR/8/34) HA-transfected HeLa cells exposed to an acidic buffer of pH 5.2 (Fig. 4). This fusion-inhibiting effect was dose-dependent with a 50% inhibitory concentration (IC_{50}) value of 12 μM. The same assay was used to determine which of the three HA mutations detected in virus resistant to compound **2** (see above) are responsible for the resistance response. In HeLa cells transfected with the HA_1-I324T mutant protein, **2** was nicely active, and the IC_{50} value was even lower compared to that of wild-type HA (Fig. 4). On the other hand, **2** was totally inactive (IC_{50} >100 μM) against the HA_1-S326V and HA_2-L99F mutants.

As demonstrated by us in a previous study [33], resistance to influenza virus fusion inhibitors can occur at two different levels. A first type of mutations, located in the inhibitor's binding pocket within HA, directly affects the HA binding capacity of the molecule. Alternatively, HA mutations that increase the fusion pH render the HA protein less stable, thereby counteracting the HA-stabilizing effect of the fusion inhibitor. This second possibility was investigated by determining the hemolysis pH of the mutant virus selected under **2**. As such, cell culture passaging without compound increased the hemolysis pH by 0.3 pH units, compared to the parent A/PR/8/34 virus grown in eggs (Table 2). Virus that arose under **2** had the same hemolysis pH (i.e., 5.3) as the no compound control, meaning that HA stability at low pH is not affected by the combination of substitutions HA_1-I324T, HA_1-S326V and HA_2-L99F.

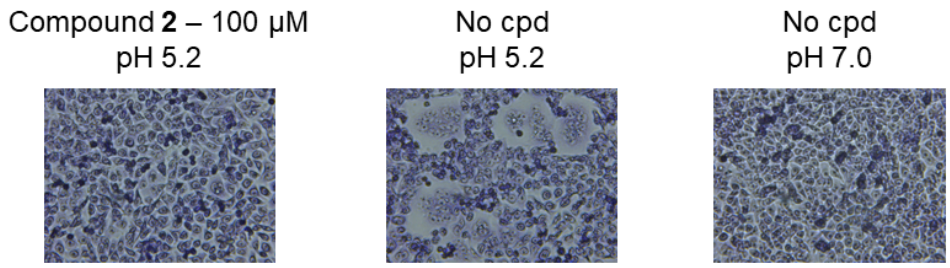

HA form (A/PR/8/34)	IC_{50} (µM) for compound 2
Wild-type	12 ± 3
HA_1-I324T	3.2 ± 0.8
HA_1-S326V	>100
HA_2-L99F	>100

Fig. 4. Inhibition of membrane fusion induced by wild-type or mutant forms of H1 HA. Compound **2** prevents polykaryon formation in HeLa cells expressing wild-type H1 HA (A/PR/8/34) and exposed to a pH 5.2 buffer. Photographs, from left to right: cells treated with 100 μM of **2** and exposed to pH 5.2; mock-treated cells exposed to pH 5.2; mock-treated cells exposed to pH 7.0. The Table shows the IC_{50} values for inhibition of polykaryon formation induced by wild-type and mutant HA proteins (mean ± SEM; N= 3).

Finally, compound **2** was further profiled by performing some additional mechanistic experiments. The potential effect on HA-mediated virus binding to sialylated cell surface glycans was evaluated in a virus binding experiment in MDCK cells kept at 4 °C. Compound **2** proved to have no effect (data not shown) whereas the sialylated lipid compound $NMSO_3$ [34], at a concentration of 200 μM, produced 96% inhibition of virus binding to MDCK cells. We also investigated whether the compounds might inhibit a cellular protease associated with influenza virus entry or HA functionality. The HA_1-I324T and HA_1-S326V substitutions in resistant virus obtained under compound **2** are lying in the cleavage loop of the HA0 precursor protein. In order to become fusion-competent, HA0 requires cleavage into its HA_1 and HA_2 polypeptides, by serine proteases trypsin and human airway trypsin-like protease (HAT) [35]. We therefore tested whether the compounds could possibly act by inhibiting these proteases (Supplementary Material Table S1). We included three cathepsin enzymes, i.e. cathepsin F used as the commercially available analogue of cathepsin W [36], a cysteine protease that was linked to endosomal escape of influenza virus by an as yet unknown mechanism [37], plus

cathepsin B and cathepsin L because of a reported link with influenza virus replication [38]. Enzymatic experiments were carried out with the methyl ester **2** as well as the free carboxylic acid that might be released intracellularly, i.e. **30**, respectively, as well as highly active compounds **31** and **34**. Neither of these molecules produced any inhibitory effect on the five proteases tested. For comparison, 1 μM of camostat gave ~90% inhibition of trypsin and HAT and the same level of inhibition was seen with 1 μM of E64 tested against cathepsin B and cathepsin L; for cathepsin F, the inhibition was ~50% (data not shown).

2.4. Structural and molecular modeling analysis

Since **2** exerts its inhibitory activity by interfering with HA-mediated membrane fusion, its potential binding to sites A and B (Fig. 1) was explored by docking computations using Glide [39, 40]. To this end, the X-ray structure of HA (H3 subtype) bound to TBHQ (PDB entry 3EYM) was used as template to generate the 3D model for A/PR/8/34 HA in an "open" conformation, which is characterized by the unfolding of the C-terminal region of helix A. This model was used to perform docking simulations in site A. On the other hand, the PDB structure 1RU7 [41] of A/PR/8/34 HA in apo form was used for the binding to site B.

Three and one main clusters were found for sites A and B, respectively, with scores ranging from -8.2 to -7.2 Kcal mol^{-1} for site A and -3.8 Kcal mol^{-1} for site B (Supplementary Material Fig. S2). In the predicted pose for **2** (cluster 1) bound to site A, the *N*-1-benzylpiperidine moiety (R_1) forms a hydrogen bond (HB) between the protonated nitrogen and the backbone oxygen of $K51_{HA2}$, and the benzylamide group (R_2) is surrounded by Leu residues at the bottom of the cavity, whereas no stabilizing interactions were observed for R_3, R_4 and R_5, which are exposed to the solvent outside the binding pocket. However, this binding mode cannot explain the SAR discussed above, such as the loss of inhibitory activity upon replacement of the benzyl moiety (R_1) by phenyl (**7**), or the changes in activity found upon chemical modifications of R_3, R_4, and R_5. In site B, **2** partially fills the hydrophobic groove formed by the HA_1 and HA_2 subunits, as the *N*-1-benzylpiperidine (R_1) and benzylamide groups (R_2) partially match some residues of the cyclic peptide CP141037. Nevertheless, no significant protein-ligand stabilizing interactions were observed, as noted in the low score of the

pose (-3.8 Kcal mol^{-1}). Furthermore, superposition of **2** with JNJ47962 revealed weak chemical resemblance in the binding motif to site B (Supplementary Material Fig. S2).

Hence, an alternative binding pocket was searched through pocket analysis using Fpocket [42]. This led to the identification of a putative binding site located at the bottom of HA in a pocket shaped by the three HA_2 helices (Fig. 5). In this pocket, **2** was anchored through several interactions (Fig. 6A), including i) a salt bridge between the protonated nitrogen of the benzylpiperidine unit (R_1) with $E120_{HA2}$, and ii) notably a direct π-stacking interaction between the benzyl ring and $F9_{HA2}$ of the fusion peptide.

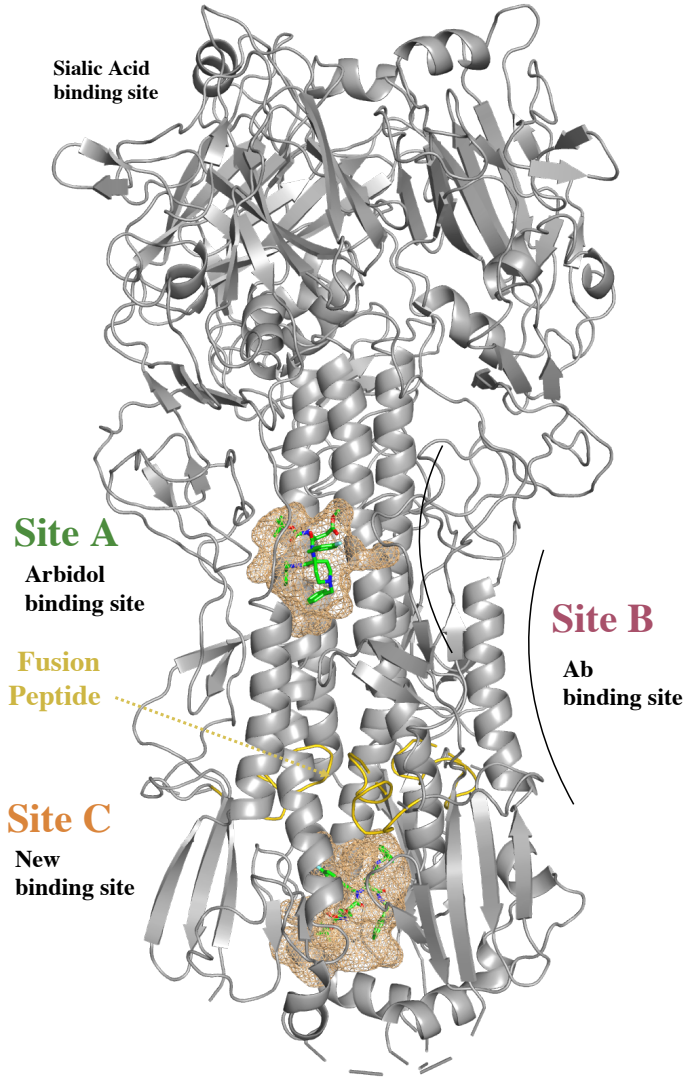

Fig. 5. Representation of the putative site proposed for the binding of compound **2** in HA.

Three independent 100 ns MD simulations were performed to investigate the structural stability of this novel HA-**2** complex. The binding mode was maintained during the simulations, as noted by the stability of the positional root-mean square deviation of both the protein and the ligand (Supplementary Material Fig. S3), and the comparison of the binding mode at the beginning and end of the simulation (Fig. 6). The salt bridge formed between the protonated piperidine of **2** and $E120_{HA2}$ is maintained in all cases, with an average N···O distance close to 3.3 Å, which is enlarged to 6.5 Å due to the insertion of a water molecule only in the last 20ns of the trajectory obtained for replica 1 (*d6* in Supplementary Material Fig. S4). Regarding the π-stacking interaction between the benzylpiperidine moiety of **2** and the benzene ring of $F9_{HA2}$, a concerted rearrangement of the aromatic rings enabled the ligand to form an additional π-stacking interaction with $Y119_{HA2}$ (Fig. 6B). The distance between the stacked aromatic rings (*d4* and *d5* in Supplementary Material Fig. S4) varied from 3.5 to 4.4 Å.

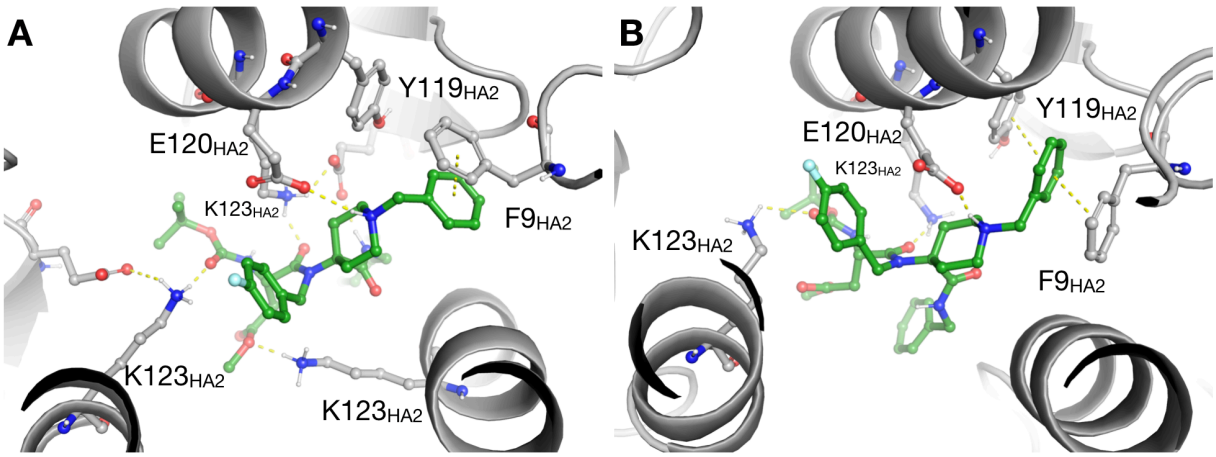

Fig. 6. Representation of (A) the energy-minimized structure of compound **2** (shown as sticks with carbon atoms coloured in green) after docking in site C of HA, and (B) the last snapshot obtained from the MD simulation of the HA-**2** complex. Selected residues involved in protein-ligand interactions are highlighted as grey sticks.

The 4-F-benzene (R_3) unit fills a cavity formed by the side chains of $K116_{HA2}$, $E120_{HA2}$, $Y119_{HA2}$, and $S124_{HA2}$ (Fig. 6; see also Supplementary Material Fig. S5 and S6). The distance of the fluorine atom in the 4-F-benzene unit to the closest atoms in these residues varies between 3.6 and 5.4 Å, suggesting a limited tolerance for accommodating larger substituents. This may explain the slight decrease in antiviral activity observed upon replacement of 4-F in **2** by 4-Me in **17** (i.e, 3.6-fold less potent), and drastic loss of activity upon substitution by 4-CF_3 in **18**, as well as the similar activity observed between **2** and its 3-F analogue (i.e., a 2.1-fold increase in EC_{50}; Table 1). Furthermore, the benzene ring of R_3 is located at around 5 Å from the protonated amino group of $K123_{HA2}$, which in turn forms a stable H-bond with the carbonyl oxygen of NH-Boc (R_4), as noted in average values of 2.9±1.0, 2.5±0.6 and 2.5±0.5 Å for the three replicas (Fig. 6).

The tight-packed arrangement of the ligand should shield the network of salt bridges formed between the protonated piperidine nitrogen of **2** and the carboxylate group of $E120_{HA2}$, which in turn is stabilized by contacts with $K116_{HA2}$, from the bulk solvent, thus reinforcing these interactions. This is reflected in the favorable binding free energy values obtained from MM/GBSA calculations, especially for replicas 1 and 3 (-24.4 ± 4.8 and -25.7 ± 4.6 Kcal mol^{-1}; Supplementary Material Table S2). Furthermore, the π-stacking of the *N*-benzyl ring with both $F9_{HA2}$ and $Y119_{HA2}$ should promote the stabilization of the fusion peptide. Remarkably, the stabilizing effect spreads up to $G1_{HA2}$ through a network of intramolecular interactions, especially involving $L2_{HA2}$, $G4_{HA2}$, $A5_{HA2}$ and $G8_{HA2}$ (Supplementary Material Fig. S7), which were identified by site-directed mutagenesis as critical for the stabilization of the fusion peptide [43]. Indeed, lower fluctuations were observed for the residues of the fusion peptide interacting with the benzyl moiety (R_1) of **2** (values of 0.87 ± 0.1, 0.89 ± 0.13 and 0.89 ± 0.1, respectively, determined for the three independent MD simulations) compared to the fluctuations of the same residues in the other two chains of HA (values of 1.0 ± 0.2/1.0 ± 0.2, 1.3 ± 0.3/1.1 ± 0.2 and 1.11 ± 0.3/1.2 ± 0.1 for monomers not involved in the π-stacking interaction; Supplementary Material Fig. S7). The key role of the *N*-1-benzylpiperidine moiety is also noted in the drastic decrease in inhibitory activity upon replacement of the benzyl group by cyclohexyl (**6**),

phenyl (**7**) or phenylethyl (**8**), since these would imply a loss of the stacking interaction, as well as by the reduced activity found upon replacement by H (**4**) or methyl (**5**).

To confirm the suitability of this binding mode, compounds **38**-**40** were rationally designed and synthesized to determine their antiviral activity (Table 1). The presence of a quaternary nitrogen in **40**, though preserving the positive charge of the ligand should affect the salt bridge with $E120_{HA2}$, leading to a drastic reduction in inhibitory activity, as confirmed experimentally (EC_{50} >100; Table 1). On the other hand, **38** and **39** were chosen to explore the ability of the benzyl ring attached to the piperidine nitrogen to fill the pocket between $F9_{HA2}$ and $Y119_{HA2}$, whose size is hindered by residues $A5_{HA2}$ and $V115_{HA2}$. Accordingly, whereas the insertion of a single F atom in *meta* position (**38**) may fill the void space between the benzene and $G134_{HA2}$, the insertion of two F atoms (**39**) would be penalized by unfavorable repulsion with the lone pairs of carbonyl oxygens in $V115_{HA2}$ and $K116_{HA2}$ (Supplementary Material Fig. S4). Indeed, the biological evaluation revealed that the antiviral activity of **2** was retained in compound **38**, but abolished in **39** (Table 1).

Finally, the suitability of this binding site is reinforced by the fact that it explains the selectivity of **2** for the A/PR/8/34 influenza virus strain and lack of activity against 2009 pandemic H1N1 virus. Thus, the HA sequence alignment of A/PR/8/34 H1N1 and A/Virginia/ATCC3/2009 H1N1 (Supplementary MaterialFig. S8) reveals the preservation of the residues that shape site C, except for replacement of $K123_{HA2}$ in A/PR/8/34 by R in A/Virginia/ATCC3/2009. Even though at first sight this appears to be a conserved mutation, this substitution in the three monomers of trimeric HA triggers a substantial reduction in the volume of the cavity, which would affect the binding of compound **2** to site C (Fig. 7). Interestingly, the analysis of HA sequences retrieved from 3DFlu [44] for different subtypes of group 1 (H1, H2, H5, H6, H8 and H9) and group 2 (H3, H7 and H10) HA proteins (Supplementary Material Fig. S9) revealed that the $K123_{HA2}R$ mutation is not only present in both HA groups, but also frequently accompanied by other changes in site C, which could explain why these compounds are specific against the H1 HA subtype (Supplementary Material Fig. S10). On the other hand, let us note that the mutation $S326_{HA1}V$, which renders the A/PR/8/34 virus and its HA

protein resistant to compound **2**, is mapped closely to the proposed new binding pocket (Supporting Information Figure S11).

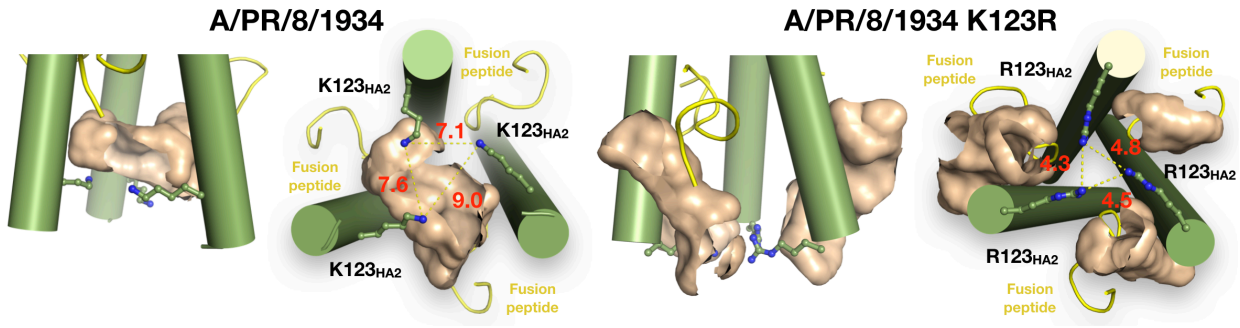

Figure 7. Representation of the cavity filled by compound **2** in site C for (left) A/PR/8/34 (determined from the last snapshot of the MD simulation), and (right) after replacement of $K123_{HA2}$ by R, reflecting the sensitivity of size and shape of site C to changes in residue composition. The fusion peptide is shown as yellow cartoon. Interatomic distances (Å) are shown in red. The cavity was determined using Fpocket.

3. Conclusion

We here report the synthesis and antiviral evaluation of 40 *N*-benzyl-4,4-disubstituted piperidines, which were easily synthesized by an Ugi four-component reaction. Several displayed low-micromolar activity against A/H1N1 influenza virus (i.e., the A/PR/8/34 strain) but not the A/H3N2 subtype. Mechanistic studies including virus resistance selection and polykaryon assays with compound **2** demonstrated that it represents a new class of H1 HA-specific membrane fusion inhibitors. The inhibitory activity is proposed to be mediated through binding to a new site in the HA_2 subunit close to the fusion peptide, which is so far unexplored to design influenza virus fusion inhibitors. Remarkably, a direct π-stacking interaction of the N_1-benzylpiperidine moiety with a $F9_{HA2}$ residue located on the fusion peptide is reinforced by the formation of a second π-stacking with $Y119_{HA2}$. The proposed binding model successfully rationalized the SAR results and the observed selectivity of **2** for the A/PR/8/34 influenza virus strain. Interestingly, the **2**-resistant HA_1-S326V mutation lies close to the new region proposed in inhibitor binding.

The antiviral efficacy of the compounds is limited to the A/PR/8/34 H1N1 virus so far, thus reducing the practical therapeutic application of this type of inhibitors. However, the unique binding mode proposed for compound **2,** which may directly stabilize the fusion peptide leading to an alternative inhibition mechanism in comparison with reported small-molecule fusion inhibitors, deserves further study. These compounds therefore appear to be promising hits, although two major challenges need to be dealt with. The first improvement would be search for chemical modifications able to form interaction with all three fusion peptides in the trimeric structure of HA, which would likely enhance the inhibitory potency. The second would be to obtain inhibition of other HA subtypes to confer broad anti-influenza A virus activity. Finally, given their direct interaction with the fusion peptide, these compounds may also serve as a scaffold to design chemical tools for exploration of the fusion process, more specifically the molecular events that occur during low pH-induced HA refolding leading to release of the fusion peptide.

4. Experimental section

4.1. Chemistry

The chemical synthesis and characterization of novel 1,4,4-trisubstituted piperidine analogues **3**, **5-11, 17-23, 25-29**, **31, 38** and **39** were carried out according to an Ugi four-component reaction as described below. The chemical synthesis and characterization of novel compound **4**, **24**, **30** and **40** were described in Supplementary Material. For **1**, **2** and the remaining piperidine compounds, the synthesis was reported in detail elsewhere [24]. The reference compounds ribavirin, chloroquine and nucleozin were from commercial sources. The sulphated sialyl lipid $NMSO_3$ was a generous gift from G. Wright (Microbiotix, Worcester, MA).

4.2. General information

Microanalytical results obtained with a Heraeus CHN-O-RAPID were within 0.4% of the theoretical values. Electrospray mass spectra were measured on a quadrupole mass spectrometer equipped with an electrospray source (Hewlett Packard, LC/MS HP 1100). Analytical thin-layer chromatography (TLC) was performed on silica gel 60 F254 (Merck). Compounds were purified by flash column

chromatography with silica gel 60 (230-400 mesh) (Merck), by preparative centrifugal circular thin-layer chromatography (CCTLC) on a Chromatotron (Kiesegel 60 PF254 gipshaltig (Merck), layer thickness of 1 mm, flow rate of 5 mL/min) or by MPLC using SNAP 12 g KP-C18-HS cartridges in an Isolera One system (Biotage). The purity of the compounds was analyzed using an analytical Agilent Technologies (model 1120 Compact LC) ACE 5 C18-300 column (150 mm x 4.6 mm). Gradient conditions were: mobile phase CH_3CN/H_2O (0.05% TFA); flow rate, 1 mL/min; detection, UV (254 and 217 nm). All retention times are quoted in minutes. HPLC–MS was performed on an HPLC Waters 2695 instrument connected to a Waters Micromass ZQ 2000 spectrometer, and a photodiode array detector. The column used was a Sunfire C18 (4.6 mmx50 mm, 3.5 mm), and the flow rate was 1 $mLmin^{-1}$. NMR spectra were recorded with Varian Inova-300, Varian Inova-400 or Varian System-500 spectrometers operating at 300, 400, or 500 MHz for ^1H NMR, and at 75, 100, or at 125 MHz for ^{13}C NMR with Me_4Si as an internal standard. The purity of novel compounds was also determined to be >95% by elemental analysis. Chemicals and reagents were obtained from commercial sources and used without further purification.

4.3.General synthetic procedure for the Ugi reaction

To a solution of the ketone (1.32 mmol) in methanol (2 mL), 2 equivalents of the corresponding amine, 2 equivalents of the amino acid and 2 equivalents of the isocyanide were successively added. The resulting mixture was stirred at room temperature for 4 days. Then, a 1.2 M solution of HCl in MeOH was added and the mixture was stirred at room temperature for 30 min. The solvent was removed under reduced pressure. The residue was redissolved in ethyl acetate and was successively washed with saturated $NaHCO_3$ (3 x 10 mL) and brine (3 x 10 mL). The organic phase was dried ($MgSO_4$), filtered and evaporated to dryness. The final residue was purified by flash column chromatography (hexane:ethyl acetate, 4:1 to 0:1) to give the novel *N*-benzyl 4,4-disubstituted piperidine analogues **3, 5-11**, **17-23**, **25-29**, **31**, **38** and **39**.

4.4. Methyl (S)-4-((1-(benzylamino)-2-methyl-1-oxopropan-2-yl)(4-fluorobenzyl)amino)-3-((tert-butoxycarbonyl)amino)-4-oxobutanoate (**3**)

Following the general procedure, a solution of acetone (0.22 mmol, 0.016 mL), 4-fluorobenzylamine (0.44 mmol, 0.071 mL), Boc-Asp(OMe)-OH (0.44 mmol, 122 mg) and benzyl isocyanide (0.44 mmol, 0.066 mL) in MeOH (2 mL) was reacted. The final residue was purified to give **3** (46 mg, 40%) as a white foam. ^{1}H NMR [500 MHz, $CDCl_3$] δ: 7.38 (dd, J = 8.5, 5.2 Hz, 2H), 7.28 (m, 6H), 7.02 (t, J = 8.5 Hz, 2H), 6.35 (d, J = 5.9 Hz, 1H), 5.08 (d, J = 9.2 Hz, 1H), 4.80 (m, 3H), 4.42 (qd, J = 14.9, 5.7 Hz, 2H), 3.47 (s, 3H), 2.79 (dd, J = 16.5, 8.9 Hz, 1H), 2.60 (dd, J = 16.5, 4.8 Hz, 1H), 1.50 (s, 3H), 1.45 (s, 3H), 1.35 (s, 9H). ^{13}C NMR [100 MHz, $CDCl_3$] δ: 174.51, 172.01, 171.97, 162.16 (d, J = 245.7 Hz), 154.62, 138.88, 133.91 (d, J = 3.3 Hz), 128.54, 128.51, 128.13, 128.07, 127.72, 127.25, 115.80 (d, J = 21.6 Hz), 80.41, 63.61, 51.90, 48.25, 47.62, 43.76, 37.72, 28.26, 25.22, 23.84. MS (ES+) m/z 530.4 $(M + 1)^+$ HPLC 9.72 min (98%) (H_2O/CH_3CN from 15/85 to 0/100 in 10 min, flow rate of 1 mL/min). Elemental analysis for $C_{28}H_{36}FN_3O$ (C, H, F, N)**:** Calculated: C, 63.50; H, 6.85; F, 3.59; N, 7.93; Found: C, 63.39; H, 6.90; F, 3.55; N, 7.92.

4.5. Methyl (S)-4-((4-(benzylcarbamoyl)-1-methylpiperidin-4-yl)(4-fluorobenzyl)amino)-3-((tert-butoxycarbonyl)amino)-4-oxobutanoate (**5**)

Following the general procedure, a solution of *N*-methylpiperidone (0.21 mmol, 0.026 mL), 4-fluorobenzylamine (0.58 mmol, 0.066 mL), Boc-Asp(OMe)-OH (143 mg,0.58 mmol)and benzyl isocyanide (0.58 mmol, 0.071 mL) in MeOH (2 mL) was reacted. The final residue was purified to give **5** (110 mg, 90%) as a white foam. ^{1}H NMR [500 MHz, $CDCl_3$] δ: 7.38-7.28 (m, 7H); 7.24 (d, J = 7.7 Hz, 2H); 6.99 (t, J = 8.4 Hz, 2H); 6.70 (t, J = 5.0 Hz, 1H); 4.99 (d, J = 9.0 Hz, 1H); 4.81-4.71 (m, 2H); 4.37 (m, 3H, 8); 3.50 (s, 3H); 2.86-2.73 (m, 4H); 2.65-2.45 (m, 2H); 2.35-2.25 (bs, 3H); 2.24-2.09 (m, 2H); 1.99-1.90 (m, 1H); 1.37 (s, 9H). ^{13}C NMR [125 MHz, $CDCl_3$] δ: 176.7, 173.2, 172.7, 171.86, 165.23, 162.3 (d, J = 246.1 Hz), 154.62, 138.8, 133.8 (d, J = 3.1 Hz), 128.6, 128.1 (d, J = 7.9 Hz, 127.7, 127.4, 116.0 (d, J = 21.6 Hz), 80.7, 64.0, 52.3, 52.0, 51.5, 49.0, 47.5, 45.0, 43.7, 37.7, 32.5, 31.5, 28.3, 23.0, 21.2. MS (ES+) m/z 586.3 $(M + 1)^+$ HPLC 3.01 min (96%) (H_2O/CH_3CN from 15/85 to 0/100 in 5 min flow rate of 1 mL/min). Anal. for $C_{31}H_{41}FN_4O_6$ (C, H, F, N): C, 63.68; H, 7.07; F, 3.25; N, 9.58. Found: C, 63.70; H, 7.05; F, 3.28; N, 9.54.

4.6. Methyl (S)-4-((4-(benzylcarbamoyl)-1-cyclohexylpiperidin-4-yl)(4-fluorobenzyl)amino)-3-((tert-butoxycarbonyl)amino)-4-oxobutanoate (**6**)

Following the general procedure, a solution of *N*-cyclohexyl-4-piperidone (0.22 mmol, 39 mg), 4-fluorobenzylamine (0.44 mmol, 0.066 mL), Boc-Asp(OMe)-OH (0.44 mmol, 122 mg) and benzyl isocyanide (0.44 mmol, 0.071 mL) in MeOH (2 mL) was reacted. The final residue was purified to give **6** (15 mg, 10%) as a white foam**.** ^{1}H NMR [400 MHz, $CDCl_3$] δ: 7.21 (m, 9H), 6.91 (t, J = 8.4 Hz, 2H), 6.73 (s, 1H), 4.95 (d, J = 9.4 Hz, 2H), 4.70 (s, 2H), 4.33 (qd, J = 14.8, 5.8 Hz, 2H), 3.48 (s, 3H), 2.58 (ddd, J = 75.6, 20.5, 10.5 Hz, 8H), 2.33 (d, J = 12.9 Hz, 2H), 2.12 (s, 2H), 1.86 (s, 2H), 1.69 (t, J = 12.6 Hz, 5H), 1.52 (d, J = 12.3 Hz, 2H), 1.11 (m, 4H). ^{13}C NMR [100 MHz, $CDCl_3$] δ: 173.36, 172.60, 171.66, 167.97, 167.62, 163.40, 154.71, 138.8 (d, J = 2.1 Hz), 134.03, 128.67, 128.13, 127.90, 127.39, 116.1 (d, J = 23 Hz), 115.83, 63.54, 52.00, 47.45, 45.64, 43.75, 29.00, 28.32, 26.01.MS (ES+) m/z 653.4 $(M + 1)^+$ HPLC 3.29 min (95%) (H_2O/CH_3CN from 15/85 to 0/100 in 5 min, flow rate of 1 mL/min). Anal. for $C_{36}H_{49}FN_4O_6$ (C, H, F, N): C, 66.24; H, 7.57; F, 2.91; N, 8.58. Found: C, 66.23; H, 7.60; F, 2.92; N, 8.55.

4.7. Methyl (S)-4-((4-(benzylcarbamoyl)-1-phenylpiperidin-4-yl)(4-fluorobenzyl)amino)-3-((tert-butoxycarbonyl)amino)-4-oxobutanoate (**7**)

Following the general procedure, a solution of *N*-phenyl-4-piperidone (37 mg, 0.21 mmol), 4-fluorobenzylamine (0.43 mmol, 0.066 mL), Boc-Asp(OMe)-OH (120 mg, 0.43 mmol) and benzyl isocyanide (0.43 mmol, 0.07 mL) in MeOH (2 mL) was reacted. The final residue was purified to give **7** (102 mg, 75%) as an orange oil. ^{1}H NMR [400 MHz, $CDCl_3$] δ: 7.40-7.12 (m, 9H), 6.95 (t, J = 8.4 HZ, 2H), 6.85-6.75 (m, 4H), 5.08 (d, J = 9.1 HZ, 1H), 4.89-4.68 (m, 3H), 4.46-4.34 (m, 2H), 3.52 (s, 3H), 3.51-3.23 (m, 3H), 3.41 (m, 5H), 3.12 (t, J = 11.5 Hz, 1H), 2.85-2.73 (m, 1H), 2.68 (d, J = 12.5 Hz, 1H), 2.63-2.52 (m, 1H), 2.41 (d, J = 12.3 Hz, 1H), 2.16-2.05 (m, 1H), 1.98-1.89 (m, 1H), 1.37 (s, 9H). ^{13}C NMR [100 MHz, $CDCl_3$] δ: 173.3, 172.7, 171.9, 162.3 (d J = 246.0 Hz), 154.8, 150.9, 138.9, 138.8 (d, J = 3.3 Hz), 129.3, 128.7, 128.2 (d, J = 8.0 Hz), 127.9, 127.5, 119.5, 116.1 (d, J = 19Hz), 80.7, 65.1, 52.1, 49.1, 47.8, 46.6, 46.1, 43.8, 37.8, 32.9, 32.1, 28.4. MS (ES+) m/z 647.8 $(M + 1)^+$ HPLC 8.2 min (95%) (H_2O/CH_3CN from 10/90 to 0/100 in 10 min, flow rate of 1 mL/min).

Anal. for $C_{36}H_{43}FN_4O_6$ (C, H, F, N): C, 66.86; H, 6.70; F, 2.94; N, 8.66. Found: C, 66.84; H, 6.72; F, 2.91; N, 8.68.

4.8. Methyl (S)-4-((4-(benzylcarbamoyl)-1-phenethylpiperidin-4-yl)(4-fluorobenzyl)amino)-3-((tert-butoxycarbonyl)amino)-4-oxobutanoate (**8**)

Following the general procedure, a solution of *N*-phenethyl-4-piperidone (0.29 mmol, 58.95 mg), 4-fluorobenzylamine (0.58 mmol, 0.066 mL), Boc-Asp(OMe)-OH (0.58 mmol, 143 mg) and benzyl isocyanide (0.58 mmol, 0.071 mL) in MeOH (2 mL) was reacted. The final residue was purified to give **8** (150 mg, 77%) as a white foam. ^{1}H NMR [500 MHz, $CDCl_3$] δ: 7.33 (m, 4H), 7.25 (m, 5H), 7.16 (m, 3H), 6.99 (t, J = 8.5 Hz, 2H), 6.76 (t, J = 5.8 Hz, 1H), 5.02 (d, J = 9.4 Hz, 1H), 4.78 (s, 2H), 4.39 (qd, J = 14.8, 5.7 Hz, 2H), 3.54 (s, 3H), 2.76 (dt, J = 26.2, 8.7 Hz, 6H), 2.58 (m, 4H), 2.39 (m, 2H), 2.02 (m, 1H), 1.86 (s, 2H), 1.37 (s, 9H). ^{13}C NMR [125 MHz, $CDCl_3$] δ: 169.22, 168.53, 167.62, 158.10 (d, J = 246.0 Hz), 150.59, 136.14, 134.73, 129.83 (d, J = 3.2 Hz), 124.68, 124.66, 124.65, 124.55, 124.53, 124.49, 124.42, 124.38, 124.06, 123.99, 123.72, 123.28, 122.09, 122.06, 111.89 (d, J = 21.5 Hz), 76.52, 60.93, 55.99, 47.90, 46.36, 45.82, 45.06, 43.44, 39.61, 33.60, 29.55, 28.98, 28.18, 25.73, 24.30, 24.23. MS (ES+) m/z 675.5 $(M + 1)^+$ HPLC 5.22 min (97%) (H_2O/CH_3CN from 15/85 to 0/100 in 10 min, flow rate of 1 mL/min). Anal. for $C_{38}H_{47}FN_4O_6$ (C, H, F, N): C, 67.64; H, 7.02; F, 2.82; N, 8.30. Found: C, 67.63; H, 7.00; F, 2.85; N, 8.32.

4.9. Methyl (S)-4-((1-benzyl-4-(cyclohexylcarbamoyl)piperidin-4-yl)(4-fluorobenzyl)amino)-3-((tert-butoxycarbonyl)amino)-4-oxobutanoate (**9**)

Following the general procedure, a solution of *N*-benzyl-4-piperidone (0.33 mmol, 0.061 mL), 4-fluorobenzylamine (0.66 mmol, 0.075 mL), Boc-Asp(OMe)-OH (0.66 mmol, 163 mg) and cyclohexyl isocyanide (0.66 mmol, 0.082 mL) in MeOH (2 mL) was reacted. The final residue was purified to give **9** (180 mg, 79%) as a white foam**.** ^{1}H NMR [500 MHz, $(CD_3)_2SO$] δ: 1.09-1.20 (m, 8H), 1.26 (s, 9H), 1.45 (m, 3H), 1.62 (m, 4H), 1.76 (m, 1H), 2.10 (m, 2H), 2.33 (m, 1H), 2.81 (m, 1H), 3.27 (m, 2H), 3.24 (m, 1H), 3.44 (s, 3H), 4.65 (m, 3H), 6.82 (d, J = 5.6 Hz, 1H),7.20 (m. 9H), 7.50 (m, 1H).^{13}C NMR [125 MHz, $(CD_3)_2SO$] δ: 171.5, 170.9, 161.3 (d, J = 242.9 Hz), 1550.3, 138.4 (d, J = 3.0 Hz), 134.9, 128.9, 128.38 (d, J = 84.6 Hz), 126.7, 115.2 (d, J = 21.9 Hz), 78.3, 63.7, 61.7,

51.5, 49.9, 49.3, 48.9, 47.5, 46.7, 28.0, 25.3, 24.8. MS (ES+) m/z 653.3 $(M + 1)^+$ HPLC 7.27 min (97%) (H_2O/CH_3CN from 15/85 to 0/100 in 10 min, flow rate of 1 mL/min). Anal. for $C_{36}H_{49}FN_4O_6$ (C, H, F, N): C, 66.24; H, 7.57; F, 2.91; N, 8.58. Found: C, 66.26; H, 7.55; F, 2.89; N, 8.60.

4.10. Methyl (S)-4-((1-benzyl-4-(tert-butylcarbamoyl)piperidin-4-yl)(4-fluorobenzyl)amino)-3-((tert-butoxycarbonyl)amino)-4-oxobutanoate (**10**)

Following the general procedure, a solution of *N*-benzyl-4-piperidone (0.33 mmol, 0.061 mL), 4-fluorobenzylamine (0.66 mmol, 0.075 mL), Boc-Asp(OMe)-OH (0.66 mmol, 163 mg) and *tert*-buthyl isocyanide (0.66 mmol, 0.079 mL) in MeOH (2 mL) was reacted. The final residue was purified to give **10** (161 mg, 74%) as a white foam**.** ^{1}H NMR [500 MHz, $(CD_3)_2SO$] δ: 7.56 (m, 2H9, 7.40 (d, J = 8.3 Hz, 1H), 7.27 (m, 3H), 7.19 (m, 5H), 6.24 (bs, 1H), 4.79 (d, J = 18.4 Hz, 1H), 4.67 (cuart., J = 7.3 Hz, 1H), 4.63 (d, J = 18.4 Hz, 1H), 3.58 (s, 3H), 2.85 (dd, J = 16.5, 6.6 Hz), 2.44 (m, 2H), 2.21 (m, 2H), 2.01 (m, 1H), 1.79 (m, 1H), 1.56 (m, 1H), 1.42 (s, 1H), 1.31 (s,)H), 1.42 (s, 1H), 1.18 (s, 9H). ^{13}C NMR [125 MHz, $(CD_3)_2SO$] δ: 171.58, 171.10, 170.96, 161.29 (d, J = 243.0 Hz), 155.02, 138.49, 135.19 (d, J = 2.9 Hz), 128.78 (d, J = 7.7 Hz), 128.69, 128.09, 128.04, 126.75, 115.34 (d, J = 21.3 Hz)78.49, 64.27, 61.80, 51.48, 49.90, 49.73, 49.17, 46.29, 36.05, 28.16, 28.04. MS (ES+) m/z 627.6 $(M + 1)^+$ HPLC 7.14 min (98%) (H_2O/CH_3CN from 15/85 to 0/100 in 10 min, flow rate of 1 mL/min). Anal. for $C_{34}H_{47}FN_4O_6$ (C, H, F, N): C, 65.16; H, 7.56; F, 3.03; N, 8.94. Found: C, 65.19; H, 7.54; F, 3.00; N, 8.90.

4.11. Methyl (S)-4-((1-benzyl-4-((tosylmethyl)carbamoyl)piperidin-4-yl)(4-fluorobenzyl)amino)-3-((tert-butoxycarbonyl)amino)-4-oxobutanoate (**11**)

Following the general procedure, a solution of *N*-benzyl-4-piperidone (0.33 mmol, 0.061 mL), 4-fluorobenzylamine (0.66 mmol, 0.075 mL), Boc-Asp(OMe)-OH (0.66 mmol, 163 mg) and *p*-toluenesulfonylmethyl isocyanide (0.66 mmol, 129 mg) in MeOH (2 mL) was reacted. The final residue was purified to give **11** (100 mg, 41%) as a white foam**.** ^{1}H NMR [500 MHz, $(CD_3)_2SO$] δ: 9.03 (m, 1H), 8.06 (bt, J = 5.8 Hz, 1H), 7.73 (d, J = 8.1 Hz, 1H), 7.68 (d, J = 8.1 Hz, 1H), 7.49 (m, 1H), 7.44 (m, 1H), 7.38 (d, J = 7.1 Hz, 2H), 7.26 (t, J = 7.3 Hz, 2H), 7.18 (m, 3H), 7.11 (d, J = 7.1 Hz, 2H), 4.55 (m, 6H), 3.55 (s, 3H), 3.16 (q, J = 13.2 Hz, 2H), 2.79 (dd, J = 16.1, 6.9 Hz, 1H), 2.46

(dd, J = 16.0, 6.9 Hz, 1H), 2.40 (s, 1H), 2.36 (s, 2H), 2.29 (d, J = 10.6 Hz, 1H), 2.22 (d, J = 10.6 Hz, 1H), 1.94 (m, 2H), 1.81 (m, 1H), 1.52 (m, 1H), 1.43 (m, 1H), 1.21 (s, 9H). ^{13}C NMR [125 MHz, $(CD_3)_2SO$] δ: 172.16, 171.44, 171.05, 161.60 (d, J = 160.4 Hz), 160.31, 154.68, 144.69, 144.41, 138.49, 134.75, 134.73 (d, J = 3.5 Hz), 129.80, 129.66, 128.53 (d, J = 6.7 Hz), 128.10, 126.78, 115.12 (d, J = 21.2 Hz), 78.51, 63.53, 61.55, 60.53, 58.53, 51.43, 49.43, 49.00, 48.93, 46.93, 36.57, 31.78, 30.92, 27.86, 21.08. MS (ES+) m/z 739.6 $(M + 1)^+$ HPLC 7.14 min (95%) (H_2O/CH_3CN from 15/85 to 0/100 in 10 min, flow rate of 1 mL/min). Anal. for $C_{38}H_{47}FN_4O_8S$ (C, H, F, N): C, 61.77; H, 6.41; F, 2.57; N, 7.58. Found: C, 61.75; H, 6.43; F, 2.60; N, 7.55.

4.12. Methyl (S)-4-((1-benzyl-4-(benzylcarbamoyl)piperidin-4-yl)(4-methylbenzyl)amino)-3-((tert-butoxycarbonyl)amino)-4-oxobutanoate (**17**)

Following the general procedure, a solution of *N*-benzyl-4-piperidone (0.21 mmol, 0.054 mL), 4-methylbenzylamine (52 mg, 0.43 mmol), Boc-Asp(OMe)-OH (119 mg, 0.43 mmol) and benzyl isocyanide (0.43 mmol, 0.06 mL) in MeOH (2 mL) was reacted. The final residue was purified to give **17** (132 mg, 95%) as an orange oil. ^{1}H NMR [400 MHz, $CDCl_3$] δ: 7.40-7.14 (m, 12H), 7.10 (t, J = 11.0 Hz, 2H), 6.71 (s, 1H), 5.12 (d, J = 9.0 Hz, 1H), 4.87-4.70 (m, 3H), 4.50-4.24 (m, 2H), 3.54 (s, 3H), 3.47-3.37 (m, 2H), 2.74 (m, 1H), 2.69-2.61 (m, 2H), 2.60-2.44 (m, 3H), 2.37 (m, 1H), 2.30 (s, 3H), 2.16 (m, 1H), 1.99 (m, 1H), 1.86 (m, 1H), 1.38 (s, 9H). ^{13}C NMR [100 MHz, $CDCl_3$] δ: 173.2, 172.9, 171.7, 154.8, 139.0, 138.7, 137.2, 135.2, 129.8, 129.3, 128.7, 128.4, 128.0, 127.4, 127.2, 126.5, 80.5, 65.3, 62.9, 52.0, 50.7, 50.1, 49.3, 48.1, 43.8, 37.8, 33.2, 32.5, 28.4, 21.3. MS (ES+) m/z 657.3 $(M + 1)^+$ HPLC 8.69 min (98%) (H_2O/CH_3CN from 15/85 to 0/100 in 10 min, flow rate of 1 mL/min). Anal. for $C_{38}H_{48}N_4O_6$ (C, H, N): C, 69.49; H, 7.37; N, 8.53. Found: C, 69.52; H, 7.35; N, 8.50.

4.13. Methyl (S)-4-((1-benzyl-4-(benzylcarbamoyl)piperidin-4-yl)(4-(trifluoromethyl)benzyl)amino)-3-((tert-butoxycarbonyl)amino)-4-oxobutanoate (**18**)

Following the general procedure, a solution of *N*-benzyl-4-piperidone (0.12 mmol, 0.025 mL), 4-(trifluoromethyl)benzylamine (0.24 mmol, 0.035 mL), Boc-Asp(OMe)-OH -OH (66.7 mg, 0.24 mmol)and benzyl isocyanide (0.24 mmol, 0.03 mL) in MeOH (2 mL) was reacted. The final residue

was purified to give **18** (81 mg, 95%) as a white foam. ^{1}H NMR [400 MHz, $CDCl_3$] δ: 7.59 (d, J = 8.2 Hz, 2H), 7.53 (d, J = 8.2 Hz, 2H), 7.39-7.21 (m, 10H), 6.82 (t, J = 4.5 Hz, 1H), 5.03 (d, J = 9.4 Hz, 1H), 4.88 (s, 2H), 4.71 (m, 1H), 4.52-4.37 (m, 2H), 3.57 (s, 3H), 3.40 (s, 2H), 2.80 (dd, J = 16.5 Hz, J = 8.6 Hz, 1H), 2.67 (m, 2H), 2.65-2.46 (m, 4H), 2.46-2.25 (m, 1H), 2.01-1.89 (m, 2H), 1.80 (m, 1H), 1.37 (s, 9H). ^{13}C NMR [100 MHz, $CDCl_3$] δ: 173.5, 172.5, 171.8, 154.7, 142.6, 138.8, 138.4, 129.31, 128.8, 128.4, 127.9, 127.5, 127.2, 126.8, 126.1 (d, J = 3.6 Hz), 80.8, 65.39, 62.9, 52.1, 50.6, 50.1, 49.2, 48.0, 43.9, 37.7, 33.2, 32.63, 28.3. MS (ES+) m/z 711.5 $(M + 1)^+$ HPLC 3.52 min (99%) (H_2O/CH_3CN from 15/85 to 0/100 in 5 min, then isocratic for 2 min; flow rate of 1 mL/min). Anal. for $C_{38}H_{45}F_3N_4O_6$ (C, H, F, N): C, 64.21; H, 6.38; F, 8.02; N, 7.88. Found: C, 64.19; H, 6.41; F, 8.00; N, 7.87.

4.14. Methyl (S)-4-((1-benzyl-4-(benzylcarbamoyl)piperidin-4-yl)(4-nitrobenzyl)amino)-3-((tert-butoxycarbonyl)amino)-4-oxobutanoate (**19**)

Following the general procedure, a solution of *N*-benzyl-4-piperidone (0.21 mmol, 0.025 mL), 4-nitrobenzylamine (66 mg, 0.43 mmol), Boc-Asp(OMe)-OH (119 mg, 0.43 mmol) and benzyl isocyanide (0.43 mmol, 0.054 mL) in MeOH (2 mL) was reacted. The final residue was purified to give **19** (124 mg, 86%) as a colourless oil**.** ^{1}H NMR [400 MHz, $CDCl_3$] δ: 8.18 (d, J = 8.6 Hz, 2H), 7.59 (d, J = 8.4 Hz, 2H), 7.41-7.15 (m, 10Hz), 6.84 (s, 1H), 5.02-4.79 (m, 2H), 4.63 (d, J = 4.0 Hz, 1H), 4.42 (d, J = 5.8 Hz, 2H), 3.56 (s, 3H), 3.41 (s, 2H), 2.8 (m, 1H), 2.67 (m, 2H), 2.55 (m, 2H), 2.43 (m, 2H), 2.28 (t, J = 11.5 Hz, 1H), 1.92 (m, 1H), 1.79 (m, 1H), 1.34 (s, 9H).^{13}C NMR [100 MHz, $CDCl_3$] δ: 173.6, 172.2, 171.8, 154.6, 147.5, 146.0, 138.7, 138.3, 129.3, 128.8, 127.9, 127.6, 127.4, 127.3, 124.3, 80.9, 65.4, 62.9, 52.2, 50.6, 50.5, 50.1, 49.3, 47.9, 43.9, 37.7, 33.2, 32.7, 28.3.MS (ES+) m/z 688.5 $(M + 1)^+$ HPLC 8.91 min (97%) (H_2O/CH_3CN from 15/85 to 0/100 in 10 min, flow rate of 1 mL/min). Anal. for $C_{37}H_{45}N_5O_8$ (C, H, N)**:** C, 64.61; H, 6.59; N, 10.18. Found: C, 64.59; H, 6.61; N, 10.17.

4.15. Methyl (S)-4-((1-benzyl-4-(benzylcarbamoyl)piperidin-4-yl)(4-chlorobenzyl)amino)-3-((tert-butoxycarbonyl)amino)-4-oxobutanoate (**20**)

Following the general procedure, a solution of *N*-benzyl-4-piperidone (0.12 mmol, 0.025 mL), 4-chlorobenzylamine (34 mg, 0.24 mmol), Boc-Asp(OMe)-OH -OH (67 mg, 0.24 mmol) and benzyl isocyanide (0.24 mmol, 0.03 mL) in MeOH (2 mL) was reacted. The final residue was purified to give **20** (70 mg, 86%) as a colourless oil. ^{1}H NMR [400 MHz, $CDCl_3$] δ: 7.49-7.09 (m, 14H), 6.74 (t, J = 5.0 Hz), 5.02 (d, J = 9.3 Hz, 1H), 4.75 (s, 2H), 4.73-4.66 (m, 1H), 4.45-4.32 (m, 2H), 3.52 (s, 3H), 3.47-3.34 (m, 2H), 2.75 (m, 1H), 2.69-2.60 (m, 2H), 2.54 (m, 3H, 2), 2.32 (m, 2H), 1.91 (m, 1H), 1.86-1.73 (m, 1H), 1.35 (s, 9H). ^{13}C NMR [100 MHz, $CDCl_3$] δ: 173.3, 172.5, 171.6, 154.5, 138.7, 138.4, 136.8, 133.3, 129.2, 129.1, 128.6, 128.3, 127.8, 127.8, 127.3, 127.1, 80.6, 65.2, 62.8, 52.0, 50.5, 49.9, 49.1, 47.6, 43.7, 37.6, 33.1, 32.4, 29.8, 28.3. MS (ES+) m/z 677.6 $(M + 1)^+$ HPLC 3.42 min (98%) (H_2O/CH_3CN from 15/85 to 0/100 in 5 min, flow rate of 1 mL/min). Anal. for $C_{37}H_{45}ClN_4O_6$ (C, H, N).C, 65.62; H, 6.70; N, 8.27. Found: C, 65.64; H, 6.69; N, 8.30.

4.16. Methyl (S)-4-((1-benzyl-4-(benzylcarbamoyl)piperidin-4-yl)(2-fluorobenzyl)amino)-3-((tert-butoxycarbonyl)amino)-4-oxobutanoate (**21**)

Following the general procedure, a solution of *N*-benzyl-4-piperidone (0.29 mmol, 0.054 mL), 2-fluorobenzylamine (0.58 mmol, 0.066 mL), Boc-Asp(OMe)-OH (0.58 mmol, 143 mg) and benzyl isocyanide (0.58 mmol, 0.071 mL) in MeOH (2 mL) was reacted. The final residue was purified to give **21** (182 mg, 95%) as a white foam.^{1}H NMR [500 MHz, $(CD_3)_2SO$] δ: .92 (bt, J = 5.9 Hz, 1H), 7.70 (m, 1H), 7.23 (m, 12 H), 7.12 (m, 2H), 4.90 (d, J = 19.0 Hz, 1H), 4.66 (m, 2H), 4.23 (d, J = 5.9 Hz, 2H), 3.52 (s, 3H), 3.35 (s, 3H), 3.27 (s, 2H), 2.79 (dd, J = 16.3, 6.0 Hz, 1H), 2.47 (m, 2H), 2.22 (m, 2H), 1.67 (td, J = 12.2, 4.2 Hz, 1H), 1.50 (m, 1H), 1.23 (s, 9H).^{13}C NMR [125 MHz, $(CD_3)_2SO$] δ: 172.14, 171.70, 170.90, 170.37, 159.07 (d, J = 243.8 Hz), 154.93, 140.04, 138.42, 129.07 (d, J = 3.4 Hz), 128.97 (d, J = 8.2 Hz), 128.69, 128.36, 128.12, 127.08, 126.81, 126.48, 125.62 (d, J = 13.2 Hz), 124.40 (d, J = 3.4 Hz), 115.26 (d, J = 21.3 Hz), 78.44, 63.54, 61.66, 59.80, 51.52, 49.70, 49.47, 49.13, 42.35, 36.44, 31.82, 27.94, 20.80, 14.12.MS (ES+) m/z 661.5 $(M + 1)^+$ HPLC 7.15 min (97%) (H_2O/CH_3CN from 15/85 to 0/100 in 10 min, flow rate of 1 mL/min). Anal. for $C_{37}H_{45}FN_4O_6$ (C, H, F, N): C, 67.25; H, 6.86; F, 2.88; N, 8.48. Found: C, 67.28; H, 6.84; F, 2.90; N, 8.45.

4.17. Methyl (S)-4-((1-benzyl-4-(benzylcarbamoyl)piperidin-4-yl)(3-fluorobenzyl)amino)-3-((tert-butoxycarbonyl)amino)-4-oxobutanoate (**22**)

Following the general procedure, a solution of *N*-benzyl-4-piperidone (0.29 mmol, 0.054 mL), 3-fluorobenzylamine (0.58 mmol, 0.066 mL), Boc-Asp(OMe)-OH (0.58 mmol, 143 mg) and benzyl isocyanide (0.58 mmol, 0.071 mL) in MeOH (2 mL) was reacted. The final residue was purified to give **22** (163 mg, 85%) as a white foam**.** ^{1}H NMR [500 MHz, $(CD_3)_2SO$] δ: 7.81 (t, J = 6.0 Hz, 1H), 7.52 (dd, J = 8.5, 5.4 Hz, 2H), 7.22 (m, 12H), 4.70 (m, 3H), 4.22 (dd, J = 5.7, 2.7 Hz, 2H), 3.52 (s, 3H), 3.34 (s, 2H), 3.27 (s, 2H), 2.79 (dd, J = 16.3, 6.0 Hz, 1H), 2.18 (m, 2H), 1.75 (dt, J = 12.8, 6.7 Hz, 1H), 1.51 (m, 1H), 1.25 (s, 9H). ^{13}C NMR [125 MHz, $(CD_3)_2SO$] δ: 172.30, 171.50, 170.96, 161.29 (d, J = 242.7 Hz), 154.95, 140.05, 138.44, 134.95 (d, J = 2.9 Hz)128.82, 128.76, 128.70, 128.36, 128.11, 127.32, 127.05, 126.64 (d, J = 41.4 Hz), 115.20 (d, J = 21.2 Hz), 78.42, 63.74, 61.66, 51.53, 49.68, 49.46, 49.07, 46.93, 42.31, 36.37, 31.96, 31.88, 27.98, 27.64, 20.81, 14.12. MS (ES+) m/z 661.9 $(M + 1)^+$ HPLC 8.32 min (98%) (H_2O/CH_3CN from 15/85 to 0/100 in 10 minflow rate of 1 mL/min). Anal. for $C_{37}H_{45}FN_4O_6$ (C, H, F, N). C, 67.25; H, 6.86; F, 2.88; N, 8.48. Found: C, 67.22; H, 6.89; F, 2.85; N, 8.50

4.18. Methyl (S)-4-((1-benzyl-4-(benzylcarbamoyl)piperidin-4-yl)(3,4-difluorobenzyl)amino)-3-((tert-butoxycarbonyl)amino)-4-oxobutanoate (**23**)

Following the general procedure, a solution of *N*-benzyl-4-piperidone (0.29 mmol, 0.054 mL), 3,4-difluorobenzylamine (0.58 mmol, 0.069 mL), Boc-Asp(OMe)-OH (0.58 mmol, 143 mg) and benzyl isocyanide (0.58 mmol, 0.071 mL) in MeOH (2 mL) was reacted. The final residue was purified to give **23** (178 mg, 90%) as a white foam. ^{1}H NMR [500 MHz, $(CD_3)_2SO$] δ: 7.86 (t, J = 6.0 Hz, 1H), 7.64 (m, 1H), 7.40 (m, 2H), 7.22 (m, 11H), 4.68 (m, 3H), 4.22 (t, J = 6.8 Hz, 2H), 3.52 (s, 3H), 3.33 (s, 1H), 3.29 (s, 2H), 2.78 (dd, J = 16.3, 6.2 Hz, 1H), 2.44 (m, 3H), 2.18 (q, J = 11.6 Hz, 2H), 1.74 (td, J = 12.6, 4.2 Hz, 1H), 1.51 (d, J = 11.0 Hz, 1H), 1.23 (s, 9H). ^{13}C NMR [125 MHz, $(CD_3)_2SO$] δ: 172.67, 171.99, 171.36, 161.46, 155.34, 150.36 (dd, J = 126.8, 12.4 Hz), 148.41 (dd, J = 126.0, 12.5 Hz), 140.44, 138.83, 137.31 (m), 129.11, 128.77, 128.54, 128.52, 127.72, 127.47, 127.32, 127.24, 126.89, 123.96 (m), 117.82 (d, J = 16.9 Hz), 116.54 (d, J = 17.8 Hz), 78.85, 64.24, 62.13, 60.21,

51.94, 50.12, 49.83, 49.47, 47.09, 42.76, 36.76, 32.40, 32.34, 28.34, 28.00, 21.22, 14.53.MS (ES+) m/z 679.9 $(M + 1)^+$ HPLC 9.01 min (97%) (H_2O/CH_3CN from 15/85 to 0/100 in 10 min, flow rate of 1 mL/min). Anal. for $C_{37}H_{44}F_2N_4O_6$ (C, H, F, N): C, 65.47; H, 6.53; F, 5.60; N, 8.25. Found: C, 65.50; H, 6.51; F, 5.58; N, 8.28.

4.19. Methyl (S)-4-((1-benzyl-4-(benzylcarbamoyl)piperidin-4-yl)(4-fluorobenzyl)amino)-4-oxobutanoate (**25**)

Following the general procedure, a solution of *N*-benzyl-4-piperidone (0.21 mmol, 0.054 mL), 4-fluorobenzylamine (0.58 mmol, 0.066 mL), mono-methyl hydrogen succinate (77 mg, 0.58 mmol) and benzyl isocyanide (0.58 mmol, 0.071 mL) in MeOH (2 mL) was reacted. The final residue was purified to give **25** (111 mg, 97%) as a colourless oil. ^{1}H NMR [500 MHz, $CDCl_3$] δ: 7.36-7.20 (m, 12H); 7.05-6.99 (m, 2H); 6.91 (ta, J = 5.2 Hz, 1H); 4.65 (s, 2H); 4.42 (d, J = 5.7 Hz, 2H); 3.63 (s, 3H); 3.41 (s, 2H); 2.72-2.6 (m, 4H); 2.61-2.50 (m, 4H); 2.32 (t, J = 11.2 Hz, 2H); 1.87 (m, 2H). ^{13}C NMR [125 MHz, $CDCl_3$] δ: 7.36-7.20 (m, 12H); 7.05-6.99 (m, 2H); 6.91 (ta, J = 5.2 Hz, 1H); 4.65 (s, 2H); 4.42 (d, J = 5.7 Hz, 2H); 3.63 (s, 3H); 3.41 (s, 2H); 2.72-2.6 (m, 4H); 2.61-2.50 (m, 4H); 2.32 (t, J = 11.2 Hz, 2H); 1.87 (m, 2H). MS (ES+) m/z 546.3 $(M + 1)^+$ HPLC 2.97 min (95%) (H_2O/CH_3CN from 15/85 to 0/100 in 5 min, flow rate of 1 mL/min). Anal. for $C_{32}H_{36}FN_3O_4$ (C, H, F, N): C, 70.44; H, 6.65; F, 3.48; N, 7.70. Found: C, 70.49; H, 6.66; F, 3.47; N, 7.69.

4.20. Methyl (S)-4-((1-benzyl-4-(benzylcarbamoyl)piperidin-4-yl)-4-fluorobenzyl)amino)-3-benzyloxycarbonylamino-4-oxobutanoate (**26**)

Following the general procedure, a solution of *N*-benzyl-4-piperidone (0.87 mmol, 0.16 mL), 4-fluorobenzylamine (1.75 mmol, 0.2 mL), Cbz-Asp(OMe)-OH (1.75 mmol, 492 mg) and benzyl isocyanide (1.75 mmol, 0.21 mL) in MeOH (2 mL) was reacted. The final residue was purified to give **26** (548 mg, 90%) as a white foam.^{1}H NMR (500 MHz, DMSO-d_6) δ 7.84 (m, 2H), 7.56 (dd, J = 8.4, 5.3 Hz, 2H), 7.39 – 7.12 (m, 15H), 5.75 (s, 1H), 5.00 (d, J = 12.5 Hz, 1H), 4.91 (d, J = 12.5 Hz, 1H), 4.83 – 4.65 (m, 3H), 4.24 (d, J = 5.7 Hz, 2H), 3.55 (s, 3H), 3.33 (m, 2H), 2.89 (dd, J = 16.7, 5.2 Hz, 1H), 2.60 – 2.52 (m, 2H), 2.22 (m, 2H), 1.79 (td, J = 12.8, 4.2 Hz, 1H), 1.50 (m, 1H). ^{13}C NMR (126 MHz, DMSO-d_6) δ 172.2, 171.3, 170.7, 161.30 (d, J = 242.8 Hz), 155.7, 139.9, 138.4, 136.7, 134.7,

134.7, 128.8, 128.74 (d, J = 7.9 Hz), 128.3, 128.1, 128.0, 127.8, 127.7, 127.0, 126.7, 126.5, 115.25 (d, J = 21.3 Hz), 65.7, 63.7, 61.6, 54.9, 51.6, 49.9, 49.7, 48.9, 46.8, 42.3, 36.0, 32.1, 31.8. MS (ES+) m/z 696.2 $(M + 1)^+$ HPLC 7.09 min (98%) (H_2O/CH_3CN from 10/90 to 0/100 in 10 min, then isocratic for 2 min; flow rate of 1 mL/min). Anal. for $C_{40}H_{43}FN_4O_6$ (C, H, F, N): C, 69.15; H, 6.24; F, 2.73; N, 8.06. Found: C, 69.17; H, 6.22; F, 2.70; N, 8.09.

4.21. tert-Butyl (S)-(1-((1-benzyl-4-(benzylcarbamoyl)piperidin-4-yl)(4-fluorobenzyl)amino)-1-oxopropan-2-yl)carbamate (**27**)

Following the general procedure, a solution of *N*-benzyl-4-piperidone (0.21 mmol, 0.054 mL), 4-fluorobenzylamine (0.58 mmol, 0.066 mL), Boc-Ala(OMe)-OH (118 mg, 0.58 mmol) and benzyl isocyanide (0.58 mmol, 0.071 mL) in MeOH (2 mL) was reacted. The final residue was purified to give **27** (126 mg, 97%) as a colourless oil. ^{1}H NMR [500 MHz, $CDCl_3$] δ: 7.33-7.10 (m, 1H); 6.97-6.80 (m, 3H, 11); 5.07 (d, J = 7.0 Hz, 1H); 4.74 (d, J = 18,2 HZ, 1H); 4.51 (d, J = 18.2 Hz, 1H); 4.32 (m, 3H); 3.33 (d, J = 13.2 Hz, 2H); 2.59 (m, 3H; 2); 2.34 (m, 2H); 2.23 (m, 1H); 1.85 (m, 2H); 1.38 (s, 9H); 1.08 (d, J = 6.6 Hz, 3H). ^{13}C NMR [125 MHz, $CDCl_3$] δ: 175.3, 171.0 , 161.0 (d, J = 246.2 Hz), 154.1 (28), 137.4, 137.1, 132.7 (d, J = 1.9 Hz), 128.1, 127.5, 127.2, 126.8 (d, J = 7.6 Hz), 126.7, 126.2, 126.0, 114.8 (d, J = 21.6 Hz), 78.8, 64.03, 61.71, 49.4, 49.1, 47.2, 46.3, 42.6, 31.8, 31.7, 27.6, 18.0. MS (ES+) m/z 603.5 $(M + 1)^+$ HPLC 3.31 min (99%) (H_2O/CH_3CN from 15/85 to 0/100 in 5 min, flow rate of 1 mL/min). Anal. for $C_{35}H_{43}FN_4O_4$ (C, H, F, N): C, 69.74; H, 7.19; F, 3.15; N, 9.30. Found: C, 69.77; H, 7.21; F, 3.13; N, 9.28.

4.22. Methyl (S)-5-((1-benzyl-4-(benzylcarbamoyl)piperidin-4-yl)(4-fluorobenzyl)amino)-4-((tert-butoxycarbonyl)amino)-5-oxopentanoate (**28**)

Following the general procedure, a solution of *N*-benzyl-4-piperidone (0.21 mmol, 0.054 mL), 4-fluorobenzylamine (0.48 mmol, 0.066 mL), Boc-Glu(OMe)-OH (0.48 mmol) and benzyl isocyanide (0.42 mmol, 0.071 mL) in MeOH (2 mL) was reacted. The final residue was purified to give **28** (72 mg, 50%) as a white foam. ^{1}H NMR [500 MHz, $CDCl_3$] δ: 8.07-7.82 (m, 4H), 7.43-7.13 (m, 7H), 6.97 (t, J = 8.2 Hz, 2H), 6.76 (bs, 1H), 5.16 (d, J = 8.0 Hz, 1H), 4.76 (m, 2H), 4.54-4.29 (m, 3H, 12), 3.59 (s, 3H), 3.43 (s, 2H), 2.69-2.55 (m, 2H), 2.45-2.20 (m, 4H), 2.00-1.78 (m, 3H), 1.66 (m, 1H),

1.46-1.29 (m, 9H). ^{13}C NMR [125 MHz, $CDCl_3$] δ: 175.0, 173.2, 172.1, 162.6, 162.1 (d, J = 246.3 Hz), 155.53, 138.5, 138.2, 133.7, 129.2, 128.7, 128.3, 128.1 (d, J = 8.1 Hz), 128.0, 127.4, 127.1, 115.94 (d, J = 21.6 Hz), 80.0, 65.2, 62.8, 51.8, 51.8, 50.43, 50.2, 47.23, 43.8, 33.0, 28.64, 28.3. MS (ES+) m/z 675.6 $(M + 1)^+$ HPLC 3.31 min (96%) (H_2O/CH_3CN from 85/15 to 5/95 in 5 min, flow rate of 1 mL/min). Anal. for $C_{38}H_{47}FN_4O_6$ (C, H, F, N): C, 67.64; H, 7.02; F, 2.82; N, 8.30. Found: C, 67.61; H, 6.99; F, 2.85; N, 8.28.

4.23. tert-Butyl (S)-(1-((1-benzyl-4-(benzylcarbamoyl)piperidin-4-yl)(4-fluorobenzyl)amino)-1-oxo-3-phenylpropan-2-yl)carbamate (**29**)

Following the general procedure, a solution of *N*-benzyl-4-piperidone (0.22 mmol, 0.054 mL), 4-fluorobenzylamine (0.44 mmol, 0.066 mL), Boc-Phe-OH (0.44 mmol, 117 mg) and benzyl isocyanide (0.44 mmol, 0.071 mL) in MeOH (2 mL) was reacted. The final residue was purified to give **29** (123 mg, 82%) as a colourless oil. ^{1}H NMR [500 MHz, $CDCl_3$] δ: 7.36 (dd, J = 8.4, 6.6 Hz, 4H), 7.26 (m, 6H), 7.01 (m, 5H), 6.89 (t, J = 8.3 Hz, 2H), 6.82 (s, 2H), 5.03 (d, J = 8.6 Hz, 1H), 4.45 (d, J = 5.7 Hz, 2H), 3.40 (t, J = 12.7 Hz, 2H), 2.99 (dd, J = 13.4, 8.0 Hz, 1H), 2.79 (d, J = 13.4 Hz, 1H), 2.75 (t, J = 6.1 Hz, 2H), 2.66 (m, 2H), 2.46 (t, J = 6.1 Hz, 2H), 2.25 (m, 2H), 1.77 (td, J = 13.0, 12.2, 4.8 Hz, 2H), 1.39 (s, 9H), 1.08 (s, 2H).^{13}C NMR [125 MHz, $CDCl_3$] δ: 209.31, 174.72, 171.85, 162.95, 161.98 (d, J = 246.0 Hz), 154.92, 138.57, 138.21, 138.15, 136.32, 133.79 (d, J = 2.9 Hz), 129.59, 129.21, 128.96, 128.67 (d, J = 3.9 Hz), 128.44, 128.26, 127.86, 127.69, 127.63, 127.41, 127.37, 127.34, 127.12, 127.08, 115.88 (d, J = 21.6 Hz), 80.10, 65.27, 62.84, 62.03, 54.04, 52.98, 50.62, 50.11, 47.08, 43.78, 41.37, 39.93, 32.86, 32.64, 28.33, 27.87. MS (ES+) m/z 679.2 $(M + 1)^+$ HPLC 3.62 min (96%) (H_2O/CH_3CN from 15/85 to 0/100 in 5 min, flow rate of 1 mL/min). Anal. for $C_{41}H_{47}FN_4O_4$ (C, H, F, N): C, 72.54; H, 6.98; F, 2.80; N, 8.25. Found: C, 72.55; H, 7.00; F, 2.78; N, 8.24.

4.24. tert-Butyl (S)-(4-amino-1-((1-benzyl-4-(benzylcarbamoyl)piperidin-4-yl)(4-fluorobenzyl)amino)-1,4-dioxobutan-2-yl)carbamate (**31**)

Following the general procedure, a solution of *N*-benzyl-4-piperidone (0.21 mmol, 0.054 mL), 4-fluorobenzylamine (0.48 mmol, 0.066 mL), Boc-Asn-OH (0.43 mmol) and benzyl isocyanide (0.42

mmol, 0.071 mL) in MeOH (2 mL) was reacted. The final residue was purified to give **31** (119 mg, 88%) as a white foam. ^{1}H NMR [500 MHz, $CDCl_3$] δ: 7.39 (s, 2H), 7.35-7.15 (m, 10H), 7.00 (t, J = 8.5 Hz, 2H), 6.66 (m, 2H), 5.94 (bs, 1H), 5.52 (bs, 1H), 4.96 (m, 2H), 4.75 (d, J = 17.8 Hz, 1H), 4.40 (m, 1H), 4.23 (m, 1H), 3.46 (m, 2H), 2.78 (m, 1H), 2.58 (m, 4H), 2.40 (m, 2H), 2.13 (m, 1H), 1.91-1.76 (m, 2H), 1.39 (s, 9H).^{13}C NMR [125 MHz,$CDCl_3$] δ: 173.9, 173.7, 172.6, 162.11 (d, J = 246.3 Hz), 155.1, 138.6, 138.1, 133.9, 129.1, 128.6, 128.4, 128.3, 127.7, 127.3, 127.1, 115.9 (d, J = 21.5 Hz), 80.3, 64.9, 62.6. MS (ES+) m/z 646.8 $(M + 1)^+$ HPLC 3.02 min (99%) (H_2O/CH_3CN from 15/85 to 0/100 in 5 min, flow rate of 1 mL/min). Anal. for $C_{36}H_{44}FN_5O_5$ (C, H, F, N): C, 66.96; H, 6.87; F, 2.94; N, 10.85. Found: C, 66.99; H, 6.85; F, 2.91; N, 10.83.

4.25. Methyl (S)-4-((4-(benzylcarbamoyl)-1-(3-fluorobenzyl)piperidin-4-yl)(4-fluorobenzyl)amino)-3-((tert-butoxycarbonyl)amino-4-oxobutanoate (**38**)

Following the general procedure, a solution of *N*-(3-fluorobenzyl)-4-piperidone (0.6 mmol, 125 mg), 4-fluorobenzylamine (1.2 mmol, 0.137 mL), Boc-Asp(OMe)-OH (1.2 mmol, 297 mg) and benzyl isocyanide (1.2 mmol, 0.146 mL) in MeOH (2 mL) was reacted. The final residue was purified to give **38** (350 mg, 86%) as a white foam ^{1}H NMR (400 MHz, DMSO-d_6) δ 7.79 (d, J = 7.7 Hz, 1H), 7.54 (dd, J = 8.5, 5.4 Hz, 2H), 7.34 – 7.15 (m, 10H), 7.06 – 6.92 (m, 3H), 4.72 (dd, J = 22.3, 7.2 Hz, 3H), 4.24 (d, J = 5.5 Hz, 2H), 3.55 (s, 3H), 3.32 (s, 2H), 2.80 (dd, J = 16.3, 6.0 Hz, 1H), 2.48 – 2.39 (m, 3H), 2.29 – 2.15 (m, 4H), 1.79 (t, J = 13.4 Hz, 1H), 1.60 – 1.52 (m, 1H), 1.27 (s, 9H).^{13}C NMR (101 MHz, DMSO) δ 172.7, 172.0, 171.4, 170.7, 162.4 (d, J = 243.1 Hz), 161.7 (d, J = 242.9 Hz), 155.4, 142.12 (d, J = 7.0 Hz), 140.4, 135.4, 130.40 (d, J = 8.3 Hz), 129.5 (d, J = 7.6 Hz),128.5, 127.5, 126.9, 124.9, 115.6 (d, J = 21.2 Hz), 115.4 (d, J = 21.0 Hz), 113.9(d, J = 21.0 Hz), 78.9, 64.2, 61.3, 60.2, 51.9, 50.1, 49.9, 49.5, 47.4, 42.8, 36.8, 32.4, 32.3, 28.4, 21.2, 14.5.MS (ES+) m/z 679.3$(M + 1)^+$ HPLC 6.78 min (99%) (H_2O/CH_3CN from 90/10 to 5/95 in 10 min flow rate of 1 mL/min). Anal. for $C_{37}H_{44}F_2N_4O_6$ (C, H, F, N): C, 65.47; H, 6.53; F, 5.60; N, 8.25. Found: C, 65.45; H, 6.50; F, 5.62; N, 8.20.

4.26. Methyl (S)-4-((4-(benzylcarbamoyl)-1-(3,5-difluorobenzyl)piperidin-4-yl)(4-fluorobenzyl)amino)-3-((tert-butoxycarbonyl)amino)-4-oxobutanoate (**39**)

Following the general procedure, a solution of *N*-(3,5-difluorobenzyl)-4-piperidone (0.6 mmol, 135 mg), 4-fluorobenzylamine (1.2 mmol, 0.137 mL), Boc-Asp(OMe)-OH (1.2 mmol, 297 mg) and benzyl isocyanide (1.2 mmol, 0.146 mL) in MeOH (2 mL) was reacted. The final residue was purified to give **39** (344 mg, 82%) as a white foam. ^{1}H NMR (400 MHz, DMSO-d_6) δ 7.80 (t, J = 5.3 Hz, 1H), 7.57 – 7.50 (m, 1H), 7.34 – 7.14 (m, 9H), 7.05 (ddd, J = 11.6, 5.8, 2.3 Hz, 1H), 6.86 (d, J = 6.6 Hz, 2H),4.72 (m, 3H), 4.23 (d, J = 5.6 Hz, 2H), 3.55 (s, 3H), 3.35 (s, 2H), 3.32 (s, 2H), 2.80 (dd, J = 16.3, 6.0 Hz, 1H), 2.44 (m, 3H), 2.23 (m, 2H), 1.81 (m, 1H), 1.56 (m, 1H), 1.27 (s, 9H). ^{13}C NMR (101 MHz, DMSO-d_6) δ 172.7, 171.9, 171.4, 170.8, 162.7 (d, J = 245.1 Hz), 163.0 (d, J = 245.2 Hz), 161.8 (d, J = 240.3 Hz), 155.4, 144.1 (t, J = 8.6 Hz), 144.0, 135.4, 129.3, 128.5, 127.5, 126.9, 115.58 (d, J = 21.2 Hz), 111.56 (d, J = 24.6 Hz), 102.58 (t, J = 25.9 Hz), 78.9, 64.1, 60.8, 60.2, 51.9, 50.0, 49.9, 49.4, 47.4, 42.8, 36.8, 32.4, 32.3, 28.4, 21.1, 14.5. MS (ES+) m/z 697.2 $(M + 1)^+$ HPLC 6.92 min (99%) (H_2O/CH_3CN from 90/10 to 5/95 in 10 min; flow rate of 1 mL/min). Anal. for $C_{37}H_{43}F_3N_4O_{66}$ (C, H, F, N): C, 63.78; H, 6.22; F, 8.18; N, 8.04. Found: C, 63.79; H, 6.20; F, 8.21; N, 8.01.

4.27. Potentiometric pKa determination

Titrations were carried out at 25 ± 0.5 °C in 0.15 M aqueous KCl solution under a nitrogen atmosphere using a SiriusT3 apparatus (Sirius Analytical Instruments Ltd, East Sussex, UK) equipped with an Ag/AgCl double junction reference pH electrode and a turbidity sensor. Standardised 0.5 M KOH and 0.5 M HCl were used as titration reagents. The KOH solution was standardized by potassium acid phthalate. The p*Ka* values are the mean of 3 titrations ± SD except otherwise noted.

4.28. Chemical stability

A solution of **2** (0.6 mg) and **34** (0.6 mg) in acetonitrile: acetate buffer (2 mL, pH=5.5) were incubed at 37 ºC for 72 h. The compounds were very stable and no degradation products were observed by HPLC and HPLC-MS in these acidic buffered solutions that may mimic the pH conditions at the endosomes.

4.29. Biological assays.

Virus strains. The panel of influenza virus strains included A/PR/8/34 (A/H1N1; ATCC® VR-95), A/Virginia/ATCC3/2009 (H1N1; ATCC® VR-1738), A/HK/7/87 (A/H3N2; a kind gift from J. Neyts, Leuven, Belgium), and and B/HK/5/72 (ATCC® VR-823). These viruses were expanded by intra-allantoic inoculation in embryonated hen eggs.

*Antiviral procedures based on reduction of virus-induced cytopathic effect***.** We previously reported [33] the cytopathic effect (CPE) reduction assay in influenza virus-infected Madin-Darby canine kidney cells (MDCK; kindly donated by M. Matrosovich, Marburg, Germany). Briefly, subconfluent cultures of MDCK cells in 96-well plates were infected with virus at an MOI of 50 $CCID_{50}$ (50% cell culture infective dose) per well, and at the same time the test compounds were added in serial dilutions. The infection medium consisted of UltraMDCK medium (Lonza), supplemented with 225 mg/L sodium bicarbonate, 2 mM L-glutamine, and 2 μg/ml TPCK (tosylphenylalanylchloromethyl-keton)-treated trypsin (Sigma-Aldrich). After 72 h incubation at 35 °C, microscopy was performed to score virus-induced CPE and compound cytotoxicity. The results were verified by a colorimetric cell viability assay. The MTS cell viability reagent (CellTiter 96® AQ_{ueous} MTS Reagent from Promega) was added to the wells, and 4 h later, absorbance at 490 nm was measured in a plate reader.

The antiviral activity of compounds was expressed as EC_{50} or concentration showing 50% effectiveness in the microscopic CPE reduction or MTS assay [see reference 45 for calculation details]. Cytotoxicity was expressed as the CC_{50} or 50% cytotoxic concentration in the MTS assay, and MCC (minimum cytotoxic concentration) or concentration producing minimal changes in cell morphology, assessed by microscopy.

Selection of resistant influenza virus mutants. MDCK cells were infected with A/PR/8/34 virus as above, and exposed to different concentrations of compound **2**. After 72 h, microscopy was done to select the highest compound concentrations manifesting some virus-induced CPE, and from these wells the cells combined with supernatants were frozen at -80°C. These harvests were further passaged in MDCK cells under gradually increasing compound concentrations until resistance was obtained (i.e. virus breakthrough at 25 μM of **2**). A no compound control condition was passaged in

parallel. Individual virus clones were obtained by plaque purification under 0.8% agar and 10 μM of **2**, followed by virus expansion in MDCK cells. After RNA extraction and reverse transcription followed by high-fidelity PCR, cycle sequencing was done on the HA gene.

Mechanistic influenza virus assays. For the one-cycle time-of-addition assay described in full detail elsewhere [28], MDCK cells were infected with influenza A/PR/8/34 virus and compounds were added at -0.5, 0, 0.5, 1, 3, 5 or 8 h p.i. At 10 h p.i., cellular RNA extracts were prepared. vRNA copy number (for the M-gene) was determined by two-step RT-qPCR using reported primers and probe [33]. The virus binding assay at 4°C was performed [28] using MDCK cells and two-step RT-qPCR quantification of cell-bound virus.

To perform the polykaryon assay [33], the coding sequence for A/PR/8/34 HA was cloned into a pCAGEN plasmid [46]. Specific HA mutations were introduced by site-directed mutagenesis and verified by cycle sequencing. Plasmid transfection into HeLa cells was carried out in 12-well plates as described [13, 33]. Two days later, surface-exposed HA0 was first activated for 15 min with TPCK-treated trypsin. Next, the cells were preincubated for 15 min with test compound; exposed for 5 min to pH 5.2 buffer [i.e. PBS with Ca^{2+} and Mg^{2+} (PBS-CM) adapted to pH 5.2 with acetic acid] with further presence of compound; and then washed with PBS-CM. Cell culture medium was added and after 3 h incubation, the cells were fixated and stained with Giemsa solution to allow microscopic counting of the polykaryons.

To measure the hemolysis pH of wild-type or mutant virus [33], virus was added to microcentrifuge tubes together with an equal volume of 2% chicken red blood cell (RBC) suspension. After 10 min incubation at 37 °C, unbound virus was removed by centrifugation. Next, the cell pellets were resuspended in acidic buffer, i.e. PBS-CM that was acidified with acetic acid to a pH ranging from 4.6 to 6 with 0.1 increments. After 25 min incubation, the suspensions were neutralized with NaOH and intact RBC were removed by centrifugation. The extent of hemolysis in the supernatants was quantified by measuring the absorbance at 540 nm using a plate reader. The hemolysis pH was defined as the pH at which 50% hemolysis occurred relative to the value at pH 4.6.

Enzymatic assays with diverse proteases. The effect of the synthesized compounds and two reference molecules, i.e. the broad cathepsin inhibitor E64 and broad serine protease inhibitor camostat, was measured in a FRET assay with 7-amino-4-methylcoumarin (AMC) fluorogenic substrates. The panel of proteases contained: trypsin (from human pancreas; Athens Research & Technology), human airway trypsin-like protease (HAT; R&D systems), and cathepsin B, cathepsin F and cathepsin L (all from Enzo Life Sciences). The assay buffers contained: for trypsin, 100 mM Tris pH 9 and 5 mg per ml bovine serum albumin; for HAT: 50 mM Tris pH 9 and 0.05% Brij-35; and for cathepsin B, F and L: 50 mM sodium acetate pH 5.5, 2.5 mM EDTA, 0.01% nia. Black 96-well plates containing serial compound dilutions were installed in a plate reader at 37 °C, and pre-incubated for 15 min with enzyme (1 pM trypsin; 1 nM HAT; 0.4 nM cathepsin L; 0.2 nM cathepsin B; or 5 nM cathepsin F). Next, the substrate (Enzo Life Sciences) was added, i.e. 50 μM and 80 μM Boc-Gln-Ala-Arg-AMC for trypsin and HAT, respectively, or 10 μM Z-Phe-Arg-AMC for cathepsin B, F and L. The rising fluorescence signal (ex: 380 nm, em: 460 nm) was monitored during 60 min.

4.30. Molecular modeling

Multiple sequence alignment. The amino acid sequence of H1N1, H1N2, H2N2, H3N2, H5N1, H6N1, H7N2, H7N3, H7N7, H7N9, H9N2, and H10N8 were aligned by using Clustal Omega (version 1.2.4; [47, 48]). A subtype multiple sequence alignment was also performed for two variants of A/PR/8 H1N1 and two variants of the pandemic A/Virginia-ATCC-2009 H1N1.

Molecular docking. Docking was performed using Glide [39, 40] with the standard precision mode to explore the potential binding of compound **2** to sites A, B, and C in A/PR/8 H1N1 HA. Docking in sites B and C was performed using the PDB structure 1RU7 of A/PR/8. For site A, the homology model of A/PR/8 in an "open" conformation (based on PDB entry 3EYM) produced in a previous work [13] was used. A cubic grid of 25 Å was applied to define each of the three binding sites. A RMSD value of 1.0 Å and an atom displacement of 2.6 were set to filter poses during clustering. A total of 50 poses were generated per ligand and four clusters were identified for each of the three analysed sites.

Molecular dynamics simulations. Amber16 [49] was used to perform MD simulations on the selected ligand–protein complex previously generated by docking analysis. The general Amber force field (GAFF) was used to parameterize the ligand [50], and the partial charges were derived at the B3LYP/6-31G(d) level, after preliminary optimization of the molecular structure, by using the restrained electrostatic potential (RESP) fitting method [51] implemented in Gaussian09 [52] and Antechamber. The A/PR/8/34 complex with compound **2** (cluster 1) obtained in site C was solvated with a truncated octahedral (TIP3P) [53] water box with a layer of 18 Å and neutralized by adding Na^+ ions. For the protein, disulphide bonds were built by using the "bond" command in tleap.

Energy minimization was accomplished in three-stages that involved firstly all hydrogen atoms, then water molecules, and finally all the system with a maximum number of minimization cycles of 10,000 for the latter stage. The minimized system was then heated from 0 to 300 K in five steps, the first being performed at constant volume and the rest at constant pressure. The system was then equilibrated for 5 ns at constant pressure. Langevin dynamics with a collision frequency of 1.0 ps-1 was applied for temperature regulation during the heating. A force constant of 10 kcal mol^{-1} $Å^{-2}$ was applied to restrain some protein-ligand contacts and thus avoid conformational distortions during heating and equilibration. These harmonic restraints were gradually eliminated during the first 50 ns of MD production. A total of 150 ns (50 for each MD replica) of un-restrained MD production was generated at constant volume and temperature in periodic boundary conditions.

The SHAKE algorithm [54] was applied to constrain bonds involving hydrogen atoms. Cut-off for non-bonded interactions was set to 10 Å. Electrostatic interactions beyond the cut-off within the periodic box were computed by applying the Particle Mesh Ewald (PME) method [55]. The weak-coupling algorithm with a time constant of 10.0 ps was used to stabilize the temperature during the simulation.

Binding free energy. MMPBSA.py was used to compute the the binding free energy of compound **2**. The method estimates the free energy (G) of the protein-ligand complex, and the separate protein and ligand as the sum of enthalpic (E_{gas}), solvation (G_{solv}) and entropic (S) terms (Eqs. 1-3).

$$G = E_{gas} + G_{solv} - TS \quad (1)$$

$$E_{gas} = E_{\text{int}} + E_{elec} + E_{vdW} \quad (2)$$

$$G_{solv} = G_{GB} + G_{SURF} \quad (3)$$

where E_{int}, E_{elec} and E_{vdW} are the internal, Coulomb and van der Waals energy components in the gas phase, G_{GB} is the polar contribution, which was evaluated by using the generalized Born solvation model, and G_{SURF} stands for the nonpolar term, which was determined using a linear dependence on the solvent-accessible surface area ($SASA$; Eq. 4).

$$G_{SURF} = \gamma SASA + b \quad (4)$$

where the surface tension (γ) is set to 0.0072 Kcal mol^{-1} Å^{-2}, and b is a correction term that was assumed to be zero in present calculations.

The binding free energy (ΔG_{bind}) was evaluated as noted in Eq. 5.

$$\Delta G_{bind} = \left\langle G_{complex} \right\rangle - \left\langle G_{protein} \right\rangle - \left\langle G_{ligand} \right\rangle \quad (5)$$

where $\left\langle G_x \right\rangle$ is the average value determined for each species (x: complex, protein, ligand) using an ensemble of 100 snapshots taken from the last 50 ns of the MD trajectory of the complex within the framework of the single-trajectory approach. The vibrational entropy term was not determined since it was assumed to cancel out in the comparison between the three complexes.

Declaration of competing interest

The authors declare that they have no known competing financial interests or personal relationships that could have appeared to influence the work reported in this paper.

Acknowledgements

L.N. acknowledges the dedicated help of Talitha Boogaerts, Leentje Persoons, Wim van Dam and Ria Van Berwaer. We thank the Spanish Government (MINECO/FEDER Project SAF2015-64629-C2, SAF2017-88107), the Consejo Superior de Investigaciones Científicas (CSIC Project 201980E028), and the Generalitat de Catalunya (2017SGR1746) for financial support. The Barcelona Supercomputer Center (BSC) is acknowledged for providing access to supercomputation resources (BCV-2019-3-0011 and BCV-2020-1-0019).

Supplementary Material

Details of chemical procedures and p*Ka* titration, biological data on activity against proteases, structural details of ligand-receptor complexes and sequence alignment, and finally NMR data and HPLC chromatograms of novel compounds (PDF). It also includes the coordinates of the structural homology model built up from PDB entry 3EYM. Molecular formula string and data (CSV) is also enclosed.

Abbreviations

Boc, *tert*-butoxycarbonyl, Cbz, benzyloxycarbonyl, CC_{50}, 50% cytotoxic concentration, CCTLC, preparative centrifugal circular thin-layer chromatography, CPE, cytopathic effect, EC_{50}, 50% effective concentration, HA, hemagglutinin, HAT, human airway trypsin-like protease, IC_{50}, 50% inhibitory concentration, MCC, minimum cytotoxic concentration, MD, molecular dynamics, MDCK, Madin-Darby canine kidney cells, MPLC, medium pressure liquid chromatography, PBS, phosphate buffered saline, PME, particle mesh Ewald method, RBC, red blood cell, SAR, structure-activity relationship, SEM, standard error of mean, TBHQ, *tert*-butylhydroxyquinone, TLC, thin layer chromatography.

References

(1) World Health Organization. Influenza (seasonal) - Fact sheet No. 211 2018. Available from: http://www.who.int/mediacentre/factsheets/fs211/en/.

(2) Neumann, G.; Noda, T.; Kawaoka, Y. Emergence and Pandemic Potential of Swine-Origin H1N1 Influenza Iirus. *Nature* **2009**, *459*, 931–939.

(3) Treanor, J. J. Clinical Practice. Influenza Vaccination. *N. Engl. J. Med*. **2016**, *375*, 1261–1268.

(4) Nguyen-Van-Tam, J. S.; Venkatesan, S.; Muthuri, S. G.; Myles, P. R. Neuraminidase Inhibitors: Who, When, Where? *Clin. Microbiol. Infect*. **2015**, *21*, 222–225.

(5) Naesens, L.; Stevaert, A.; Vanderlinden, E. Antiviral Therapies on the Horizon for Influenza. *Curr. Opin. Pharmacol*. **2016**, *30*, 106–115.

(6) Stevaert, A.; Naesens, L. The Influenza Virus Polymerase Complex: An Update on Its Structure, Functions, and Significance for Antiviral Drug Design. *Med. Res. Rev*. **2016**, *36*, 1127–1173.

(7) Vanderlinden, E.; Naesens, L. Emerging Antiviral Strategies to Interfere with Influenza Virus Entry. *Med. Res. Rev*. **2014**, *34*, 301–339.

(8) Byrd-Leotis, L.; Cummings, R. D.; Steinhauer, D. A. The Interplay Between the Host Receptor and Influenza Virus Hemagglutinin and Neuraminidase. *Int. J. Mol. Sci*. **2017**, *18*, e1541.

(9) Li, F.; Ma, C.; Wang, J. Inhibitors Targeting the Influenza Virus Hemagglutinin. *Curr. Med. Chem*. **2015**, *22*, 1361–1382.

(10) Russell, R. J.; Kerry, P. S.; Stevens, D. J.; Steinhauer, D. A.; Martin, S. R.; Gamblin, S. J.; Skehel, J. J. Structure of Influenza Hemagglutinin in Complex with an Inhibitor of Membrane Fusion. *Proc. Natl. Acad. Sci. U. S. A*. **2008**, *105*, 17736–17741.

(11) Kadam, R. U.; Wilson, I. A. Structural Basis of Influenza Virus Fusion Inhibition by the Antiviral Drug Arbidol. *Proc. Natl. Acad. Sci. U. S. A*. **2016**, *114*, 206–214.

(12) Kadam, R. U.; Wilson, I. A. A Small-Molecule Fragment that Emulates Binding of Receptor and Broadly Neutralizing Antibodies to Influenza A Hemagglutinin. *Proc. Natl. Acad. Sci. U. S. A*. **2018**, **115**, 4240–4245.

(13) Leiva, R.; Barniol-Xicota, M.; Codony, S, Ginex, T.; Vanderlinden, E.; Montes, M.; Caffrey, M.; Luque, F. J.; Naesens, L.; Vázquez, S. Aniline-Based Inhibitors of Influenza H1N1 Virus Acting on Hemagglutinin-Mediated Fusion. *J. Med. Chem*. **2018**, *61*, 98–118.

(14) van Dongen, M. J. P.; Kadam, R. U.; Juraszek, J.; Lawson, E.; Brandenburg, B.; Schmitz, F.; Schepens, W. B. G.; Stoops, B.; van Diepen, H. A.; Jongeneelen, M.; Tang, C, Vermond, J.; van Eijgen-Obregoso Real, A.; Blokland, S.; Garg, D.; Yu, W.; Goutier, W.; Lanckacker, E.; Klap, J. M.; Peeters, D. C. G.; Wu, J.; Buyck, C.; Jonckers, T. H. M.; Roymans, D.; Roevens, P.; Vogels, R.; Koudstaal, W.; Friesen, R. H. E.; Raboisson, P.; Dhanak, D.; Goudsmit, J.; Wilson, I. A. A Small-Molecule Fusion Inhibitor of Influenza Virus is Orally Active in Mice. *Science* **2019**, 363, eaar6221.

(15) Kadam, R. U.; Juraszek, J.; Brandenburg, B.; Buyck, C.; Schepens, W. B. G.; Kesteleyn, B.; Stoops, B.; Vreeken, R. J.; Vermond, J.; Goutier, W.; Tang, C.; Vogels, R.; Friesen, R. H. E.; Goudsmit, J.; van Dongen, M. J. P.; Wilson, I. A. Potent Peptidic Fusion Inhibitors of Influenza Virus. *Science* **2017**, *358*, 496–502.

(16) Basu, A.; Antanasijevic, A.; Wang, M.; Li, B.; Mills, D. M.; Ames, J. A.; Nash, P. J.; Williams, J. D.; Peet, N. P.; Moir, D. T.; Prichard, M. N.; Keith, K. A.; Barnard, D. L.; Caffrey, M.; Rong, L.; Bowlin, T. L. New Small Molecule Entry Inhibitors Targeting Hemagglutinin-Mediated Influenza A Virus Fusion. *J. Virol*. **2014**, *88*, 1447–1460.

(17) For a recent monograph about piperidine in medicinal chemistry, see: Vardanyan, R. *Piperidine-Based Drug Discovery*, 1st ed.; Elsevier: Amsterdam, 2017.

(18) For a recent review on anticancer, see: Goel, P.; Alam, N.; Naim, M. J.; Nawz, F.; Iqbal, M.; Alam, M. I. Recent Advancement of Piperidine Moiety in Treatment of Cancer -A Review. *Eur. J. Med. Chem*. **2018**, *157*, 480–502.

(19) Yamada; K.; Brousseau, M.; Honma, W.; Iimura, A.; Imase, H. et al Discovery of a Novel Piperidine-Based Inhibitor of Cholesteryl Ester Transfer Protein (CETP) That Retains Activity in Hypertriglyceridemic Plasma, *J. Med. Chem*. **2017**, *60*, 8466-8481.

(20) Seth, A.; Sharma, P. A.; Tripathi, A.; Choubey, P. K.; Srivastava, P.; Tripathi, P. N.; Shrivastava, S. K. Design, Synthesis, Evaluation and Molecular Modeling Studies of Some Novel N-

Substituted Piperidine-3-Carboxylic Acid Derivatives as Potential Antocinvulsants. *Med. Chem. Res.* **2018**, *27*, 1206–1225.

(21) Lv, K.; Tao, Z.; Liu, Q.; Yang, L.; Wang, B.; Wu, S.; Wang, A.; Huang, M.; Liu, M.; Lu, Y. Design, Synthesis and Antitubercular Evaluation of Benzothiazinones Containing a Piperidine Moiety. *Eur. J. Med. Chem*. **2018**, *151*, 1–8.

(22) Li, X.; Gao, P.; Huang, B.; Zhou, Z.; Yu, Z.; Yuan, Z.; Liu, H.; Pannecouque, C.; Daelemans, D.; De Clerq, E.; Zhan, P.; Liu, X. Discovery of Novel Piperidine-Substituted Indolylarylsulfones as Potent HIV NNRTIs via Structure-Guided Scaffold Morphing and Fragment Rearrangement. *Eur. J. Med. Chem*. **2017**, *126*, 190–201.

(23) Taylor, R. D.; MacCoss, M.; Lawson, A. D. G. Rings in Drugs. *J. Med. Chem.* **2014**, *57*, 5845–5859.

(24) De Castro S.; Camarasa M. J.; Balzarini J.; Velazquez S. Discovery and SAR Studies of a Novel Class of Cytotoxic 1,4-Disubstituted Piperidines Via Ugi Reaction. *Eur. J. Med. Chem.* **2014**, *83*, 174-189.

(25) Dömling, A., Ugi, I. Multicomponent Reactions with Isocyanides. *Angew. Chem. Int. Ed.* **2000**, *39*, 3168–3210.

(26) Biggs-Houck, J. E., Younai, A., Shaw, J. T. Recent Advances in Multicomponent Reactions for Diversity-Oriented Synthesis. *Curr. Opin. Chem. Biol.* **2010**, *14*, 371–382.

(27) Akritopoulou-Zanze, I. Isocyanide-Based Multicomponent Reactions in Drug Discovery. *Curr. Opin. Chem. Biol.* **2008**, *12*, 324–331.

(28) Vanderlinden, E.; Vanstreels, E.; Boons, E.; ter Veer, W.; Huckriede, A.; Daelemans, D.; van Lommel, A.; Röth, E.; Sztaricskai, F.; Herczegh, P.; Naesens, L. Intracytoplasmic trapping of influenza virus by a lipophilic derivative of aglycoristocetin. *J. Virol*. **2012**, *86*, 9416–9431.

(29) Vanderlinden, E.; Vrancken, B.; Van Houdt, J.; Rajwanshi, V. K.; Gillemot, S.; Andrei, G.; Lemey, P.; Naesens, L. Distinct Effects of T-705 (Favipiravir) and Ribavirin on Influenza Virus Replication and Viral RNA Synthesis. *Antimicrob. Agents Chemother*. **2016**, *60*, 6679–6691.

(30) Amorim, M. J.; Kao, R. Y.; Digard, P. Nucleozin Targets Cytoplasmic Trafficking of Viral Ribonucleoprotein-Rab11 Complexes in Influenza A Virus Infection. *J. Virol*. **2013**, *87*, 4694–4703.

(31) Stauffer, S.; Feng, Y.; Nebioglu, F.; Heilig, R.; Picotti, P.; Helenius, A. Stepwise Priming by Acidic pH and a High K^+ Concentration is Required for Efficient Uncoating of Influenza A Virus Cores After Penetration. *J. Virol*. **2014**, *88*, 13029–13046.

(32) Torres, E.; Duque, M. D.; Vanderlinden, E.; Ma, C.; Pinto, L. H.; Camps, P.; Froeyen, M.; Vázquez, S.; Naesens, L. Role of the Viral Hemagglutinin in the Anti-Influenza Virus Activity of Newly Synthesized Polycyclic Amine Compounds. *Antiviral Res*. **2013**, *99*, 281–291.

(33) Vanderlinden, E.; Göktas, F.; Cesur, Z.; Froeyen, M.; Reed, M. L.; Russell C. J.; Cesur, N.; Naesens, L. Novel Inhibitors of Influenza Virus Fusion: Structure-Activity Relationship and Interaction with the Viral Hemagglutinin. *J. Virol*. **2010**, *84*, 4277–4288.

(34) Kimura, K.; Mori, S.; Tomita, K.; Ohno, K.; Takahashi, K.; Shigeta, S.; Terada, M. Antiviral Activity of NMSO3 Against Respiratory Syncytial Virus Infection in Vitro and in Vivo. *Antiviral Res*. **2000**, *47*, 41–51.

(35) Laporte, M.; Naesens, L. Airway Proteases: an Emerging Drug Target for Influenza and Other Respiratory Virus Infections. *Curr*. *Opin*. *Virol*. **2017**, *24*,16–24.

(36) Santamaria, I.; Velasco, G.; Pendas, A. M.; Paz, A.; Lopez-Otin, C. Molecular Cloning and Structural and Functional Characterization of Human Cathepsin F, a New Cysteine Proteinase of the Papain Family with a Long Propeptide Domain. *J. Biol. Chem*. **1999**, *274*, 13800–13809.

(37) Edinger, T. O.; Pohl, M. O.; Yanguez, E.; Stertz, S. Cathepsin W is Required for Escape of Influenza A Virus from Late Endosomes. *MBio* **2015**, *6*, e00297.

(38) Coleman, M. D.; Ha, S. D.; Haeryfar, S. M. M.; Barr, S. D.; Kim, SO. Cathepsin B Plays a Key Role in Optimal Production of the Influenza A Virus. *J. Virol. Antivir. Res*. **2018**, *2018*, 1–20.

(39) Halgren, T. A.; Murphy, R. B.; Friesner, R. A.; Beard, H. S.; Frye, L. L.; Pollard, W. T.; Banks, J. L. Glide: A New Approach for Rapid, Accurate Docking and Scoring. 2. Enrichment Factors in Database Screening. *J. Med. Chem*. **2004**, *47*, 1750-1759.

(40) Friesner, R. A.; Banks, J. L.; Murphy, R. B.; Halgren, T. A.; Klicic, J. J.; Mainz, D. T.; Repasky, M. P.; Knoll, E. H.; Shaw, D. E.; Shelley, M.; Perry, J. K.; Francis, P.; Shenkin, P. S. Glide: A New Approach for Rapid, Accurate Docking and Scoring. 1. Method and Assessment of Docking Accuracy. *J Med. Chem*. **2004**, *47*, 1739–1749.

(41) Gamblin, S. J.; Haire, L. F.; Russell, R. J.; Stevens, D. J.; Xiao, B.; Ha, Y.; Vasisht, N.; Steinhauer, D. A.; Daniels, R. S.; Elliot, A.; Wiley, D. C.; Skehel, J. J. The Structure and Receptor Binding Properties of the 1918 Influenza Hemagglutinin. *Science* **2004**, *303*, 1838–1842.

(42) Le Guilloux, V.; Schmidtke, P.; Tuffery, P. Fpocket: A Open Source Platform for Ligand Pocket Detection. *BMC Bioinformatics* **2009**, *10*, 168.

(43) Skehel J. J.; Wiley D. C. Receptor binding and membrane fusion in virus entry: the influenza hemagglutinin. *Annu. Rev. Biochem.* **2000**, *69*, 531-569.

(44) Mazzocco, G.; Lazniewski, M.; Migdal, P.; Szczepinska, T.; Radomski, J. P.; Plewczynski, D. 3DFlu: Database of Sequence and Structural Variability of the Influenza Hemagglutinin at Population Scale. *Database* **2016**, baw130.

(45) Vrijens, P.; Noppen, S.; Boogaerts, T.; Vanstreels, E.; Ronca, R.; Chiodelli, P.; Laporte, M.; Vanderlinden, E.; Liekens, S.; Stevaert, A.; Naesens, L. Influenza virus entry via the GM3 ganglioside-mediated platelet-derived growth factor receptor beta signalling pathway. *J. Gen. Virol.* **2019**, *100*, 583-601.

(46) Matsuda, T.; Cepko, C. Electroporation and RNA interference in the rodent retina in vivo and in vitro. *Proc. Natl. Acad. Sci. U. S. A*. **2004**, *101*, 16-22.

(47) Sievers, F.; Wilm, A.; Dineen, D. G.; Gibson, T. J.; Karplus, K.; Li, W.; Lopez, R.; McWilliam, H.; Remmert, M.; Söding, J.; Thompson, J. D.; Higgins, D. G. Fast, Scalable Generation of High-Quality Protein Multiple Sequence Alignments Using Clustal Omega. *Mol. Syst. Biol*. **2011**, *7*, 539-544.

(48) Sievers, F.; Higgins, D. G. Clustal Omega for Making Accurate Alignments of Many Protein Sequences. *Protein Sci*. **2018**, *27*, 135–145.

(49) Case, D. A.; Betz, R. M.; Cerutti, D. S.; Cheatham, T. E., III; Darden, T. A.; Duke, R. E.; Giese, T. J.; Gohlke, H.; Goetz, A. W.; Homeyer, N.; Izadi, S.; Janowski, P.; Kaus, J.; Kovalenko, A.; Lee, T. S.; LeGrand, S.: Li, P.; Lin, C.; Luchko, T.; Luo, R.; Madej, B.; Mermelstein, D.; Merz, K. M.; Monard, G.; Nguyen, H.; Nguyen, H. T.; Omelyan, I.; Onufriev, A.; Roe, D. R.; Roitberg, A.; Sagui, C.; Simmerling, C. L.; Botello-Smith, W. M.; Swails, J.; Walker, R. C.; Wang, J.; Wolf, R. M.; Wu, X.; Xiao. L.; Kollman, P. A. AMBER 2016, University of California, San Francisco.

(50) Wang, J.; Wolf, R. M.; Caldwell, J. W.; Kollman, P. A.; Case, D. A. Development and Testing of a General Amber Force Field. *J. Comput. Chem.* **2004**, *25*, 1157-1174.

(51) Wang, J.; Cieplak, P.; Kollman, P. A. How Well Does a Restrained Electrostatic Potential (RESP) Model Perform in Calculating Conformational Energies of Organic and Biological Molecules? *J. Comput. Chem.* **2000**, *21*, 1049-1074.

(52) Gaussian 09, Revision E.01, Frisch, M. J.; Trucks, G. W.; Schlegel, H. B.; Scuseria, G. E.; Robb, M. A.; Cheeseman, J. R.; Scalmani, G.; Barone, V.; Mennucci, B.; Petersson, G. A.; Nakatsuji, H.; Caricato, M.; Li, X.; Hratchian, H. P.; Izmaylov, A. F.; Bloino, J.; Zheng, G.; Sonnenberg, J. L.; Hada, M.; Ehara, M.; Toyota, K.; Fukuda, R.; Hasegawa, J.; Ishida, M.; Nakajima, T.; Honda, Y.; Kitao, O.; Nakai, H.; Vreven, T.; Montgomery, J. A., Jr.; Peralta, J. E.; Ogliaro, F.; Bearpark, M.; Heyd, J. J.; Brothers, E.; Kudin, K. N.; Staroverov, V. N.; Kobayashi, R.; Normand, J.; Raghavachari, K.; Rendell, A.; Burant, J. C.; Iyengar, S. S.; Tomasi, J.; Cossi, M.; Rega, N.; Millam, J. M.; Klene, M.; Knox, J. E.; Cross, J. B.; Bakken, V.; Adamo, C.; Jaramillo, J.; Gomperts, R.; Stratmann, R. E.; Yazyev, O.; Austin, A. J.; Cammi, R.; Pomelli, C.; Ochterski, J. W.; Martin, R. L.; Morokuma, K.; Zakrzewski, V. G.; Voth, G. A.; Salvador, P.; Dannenberg, J. J.; Dapprich, S.; Daniels, A. D.; Farkas, Ö.; Foresman, J. B.; Ortiz, J. V.; Cioslowski, J.; Fox, D. J. Gaussian, Inc., Wallingford CT, 2009.

(53) Jorgensen, W. L.; Chandrasekhar, J.; Madura, J. D.; Impey, R. W.; Klein, M. L. Comparison of Simple Potential Functions for Simulating Liquid Water. *J. Chem. Phys*. **1983**, *79*, 926-935.

(54) Ryckaert, J.-P.; Ciccotti, G.; Berendsen, H. J. C. Numerical Integration fo the Cartesian Equations of Motion of a System with Constraints: Molecular Dynamics of n-Alkanes. *J. Comput. Phys.* **1977**, *23*, 327-341.

(55) Darden, T.; York, D.; Pedersen, L. An N.log(N) Method for Ewald Sums in Large Systems. *J. Chem. Phys*. **1993**, *98*, 10089-1092.

Graphical Abstract